Journal of Polymers and the Environment (2022) 30:5024–5048
https://doi.org/10.1007/s10924-022-02573-4

ORIGINAL PAPER

Cationic Surfactant-Modified Cellulose Nanocrystal/Alginate Hydrogel Beads for Enhanced Adsorptive Removal of 4-Chlorophenol from Wastewater

Tuan Sherwyn Hamidon[1] · Rohana Adnan[1] · M. K. Mohamad Haafiz[2] · M. Hazwan Hussin[1]

Accepted: 25 August 2022 / Published online: 8 September 2022

Abstract
4-Chlorophenol being a phenolic endocrine-disrupting chemical is one of the most commonly detected pollutants in water resources, which is well known for its high toxicity and carcinogenicity. The present study aimed to develop cost-effective and efficient hydrogel beads in treating wastewater contaminated with 4-chlorophenol. Herein, cetyltrimethylammonium chloride-modified cellulose nanocrystals were grafted onto the backbone of alginate to fabricate porous eco-friendly hydrogel beads (CTAC-CNC/ALG@HB) to utilize as an adsorbent. Porous CTAC-CNC/ALG@HB were characterized by Fourier transform infrared spectroscopy, scanning electron microscopy, thermogravimetric analysis, X-ray photoelectron spectroscopy, surface area/porosity measurement, and zeta potential analysis. Characterization results revealed that cetyltrimethylammonium chloride modification and the disintegration of calcium phosphate within the hydrogel beads enhanced the pore network and its structural stability. The adsorptive removal of 4-CP was optimized by altering various experimental conditions. The pseudo-second-order rate equation and the Langmuir adsorption isotherm best described the adsorption of 4-chlorophenol onto CTAC-CNC/ALG@HB. The maximum adsorption capacity was 64.935 mg g^{-1}, which could be reused up to five repeated cycles. The thermodynamic study indicated that the adsorption process was exothermic, spontaneous, and reversible within the analyzed temperature range. The Weber–Morris model revealed that intraparticle diffusion was not the singular rate-controlling step in the adsorption process. The results revealed that CTAC-CNC/ALG@HB could be employed as a sustainable and effective adsorbent for 4-chlorophenol remediation.

Keywords Cellulose nanocrystal · Cationic surfactant modification · Alginate biopolymer matrix · Wastewater treatment · 4-Chlorophenol · Regeneration

Introduction

Water is one of the vital sources for the persistent affluence of developed and developing nations; hence enhancing the ecological prominence of water supplies is an emergent topic of emphasis, especially among environmental researchers [1]. Rapid urbanization and industrialization have provoked increasing demand for clean water due to ubiquitous contaminations in environmental water [2]. It is well known that wastewater effluents contaminate surface and groundwater bodies from various sources, including industrial, medical, municipal, domestic and agricultural sectors [3]. In particular, chemical and petrochemical industries generate massive amounts of organic contaminants, prone to bioaccumulating, hence instigating an undesirable impact on access to drinkable water [4]. 4-Chlorophenol, a phenolic endocrine-disrupting chemical, is one of the most commonly detected pollutants in water streams, well-known for its high toxicity and carcinogenicity [5]. It has been reported that long-term consumption of chlorophenol-adulterated water stimulates particularly anemia and dizziness, among other symptoms, and can even affect the central nervous system and liver [6]. Although most of the chlorophenols are biorefractory pollutants, they have been extensively exploited as preservatives in wood, fibers, paints, and leather industries,

✉ M. Hazwan Hussin
mhh@usm.my; mhh.usm@gmail.com

[1] Materials Technology Research Group (MaTReC), School of Chemical Sciences, Universiti Sains Malaysia, 11800 Minden, Penang, Malaysia

[2] School of Industrial Technology, Universiti Sains Malaysia, 11800 Minden, Penang, Malaysia

used as disinfectants, as well as utilized in the industrial production of preservatives, herbicides, pesticides, phenolic resins and dyes, which consequently end up in water resources [7].

Globally, organic wastewater remediation persists as a severe concern up until now, regardless of numerous technological developments and discoveries. Different standard remediation technologies have been developed to detoxify phenolic compounds from industrial wastewater, groundwater, lakes, and rivers. However, adsorption has been the most widely employed technique for organic pollutants' removal in wastewater by dint of several shortcomings inherent to conventional methodologies, such as inefficient removal, high energy demand, expensive disposal practices and tricky operating conditions [8, 9]. The extensive application of activated carbon as a remediation agent is limited because of the high production cost, relatively high energy demand during production and regeneration, and rigorous constraints concerning the pH range of wastewater. These reasons have persuaded researchers to develop non-conventional adsorbents which are cost-effective and highly efficient at the same time in detoxifying contaminants, even in trace amounts [10].

Most natural waste biomaterials do not offer high adsorption performance due to relatively low specific surface area and undesirable uptake capacity. On the other hand, nanomaterials comprise distinctive chemical and physical properties and have primarily been exploited as nano-adsorbents in recent years. It is well known that nanocellulose-based beads provide considerable benefits over commercial adsorbents for water pollution control in terms of production cost, wide source, reusability, reactivity, biodegradability, and sludge production [3, 11, 12]. Since adsorbents should possess an easy separation from wastewater and should be easily regenerated with a minimum loss in the adsorption capacity, adsorbents need to be prepared in the form of beads [13]. Among the nano-adsorbents, cellulose nanocrystals (CNCs) offer eco-friendly and sustainable wastewater-purification treatment pertaining to its many advantages, and CNCs do not generate hazardous by-products [11]. CNC is a derivative of cellulose, the most abundant renewable natural biopolymer available on Earth; hence it is affordable [14, 15]. Moreover, the presence of reactive hydroxyl groups permits grafting of numerous functional chemical species to customize the surface properties for adsorption efficiency and adsorption capacity enhancement [16].

Cellulose nanocrystals produced through acid hydrolysis are negatively charged, hence 4-CP adsorption cannot proceed through electrostatic attraction. Many surface modification techniques including polymer grafting, use of coupling agents, and acetylation destruct the nanostructure of CNC and employs toxic solvents to achieve the chemical modification. However, nanocellulose modified with cationic surfactants not only impart a positively charged surface, but also offer convenience of preparation, ease of control and preserve the morphology of nanocellulose [17]. Surfactants are indispensable at a commercial scale as emulsifying, dispersing, and cleaning agents [18], while trimethylammonium-based surfactants are explicitly employed in the textile and medical industries [19]. Many commercially available trimethylammonium-based surfactants are also employed as the main active ingredient in household chemicals (conditioning shampoos and hair styling products) and cosmetic industries [20]. Cetyltrimethylammonium chloride (CTAC) used in the present study is a renewable and a sustainable quaternary ammonium cationic surfactant, which not only introduces a positive surface charge to CNC-based hydrogel beads to improve its hydrophobic properties, but CTAC is also nonpetroleum-based, bearing least environmental impact and functions as a dispersant to prevent the aggregation of CNCs.

Valorization of low-cost agricultural wastes and crops is an eminent topic of interest at present. Herein, oil palm fronds (OPF), an agricultural waste derived from one of the most value-added commercial crops, were used to extract CNCs. To the best of our knowledge and understanding, no comprehensive research studies elaborate on the adsorptive removal performance of CTAC modified-cellulose nanocrystal based alginate hydrogel beads for 4-chlorophenol remediation in wastewater. Hence, this study's overarching objective was to engage a facile approach to develop novel and sturdy porous cetyltrimethylammonium chloride-modified cellulose nanocrystal/alginate hydrogel beads for 4-chlorophenol adsorption. Modified CNCs were integrated with sodium alginate to formulate hydrogel beads for easy separation following adsorption and enhance the thermal stability and recyclability of porous CTAC-CNC/ALG@HB. The formulation comprised different CNC and ALG mass ratios to ascertain the optimum CNC and ALG combination. CTAC-CNC/ALG@HB was prepared through ionotropic gelation of sodium alginate, CNC, and calcium phosphate with Ca^{2+} ions and was characterized via different analytical techniques. The maximum adsorption efficiency of 4-chlorophenol on CTAC-CNC/ALG@HB was examined using numerous operating parameters. Thermodynamics of adsorption, adsorption isotherms and adsorption kinetics were also adopted to elucidate the interaction mechanism between CTAC-CNC/ALG@HB and 4-chlorophenol.

Experimental

Materials and Chemical Reagents

Fresh oil palm (*Elaeis guineensis* Jacq.) fronds obtained from an oil palm plantation in Pulau Pinang, Malaysia were

used as the raw material. 4-Chlorophenol (≥ 99%), cetyltrimethylammonium chloride (≥ 98% NT), sodium alginate, sodium monohydrogen phosphate and dialysis tubing cellulose membrane (avg. flat width 33 mm) were purchased from Sigma-Aldrich (USA), while sulphuric acid (98%) was acquired from J.T. Baker, USA. Sodium chlorite (80%) was supplied by Acros Organics (USA), whereas toluene (99.5%), ethanol (96%), glacial acetic acid (99.8%), hydrochloric acid (37%) and sodium hydroxide pellet (98%) were provided by QRëC, Malaysia. Anhydrous calcium chloride (96%) was procured from Bendosen, UK. All chemicals used were of analytical grade and used without further purification.

Fabrication of Porous CTAC-CNC/ALG Hydrogel Beads

Cellulose nanocrystals were produced from α-cellulose extracted from OPF (CNC-OPF), applying the sulfuric acid treatment adopted by Melikoğlu and co-workers [21] with a few modifications. The preparation details of CNC-OPF have been mentioned in E-supplementary data. Prior to the modification process, a CNC suspension of 1.25% (w/v) was brought to pH 10 with 0.1 M NaOH solution. The CNC suspension was then added dropwise into the CTAC solution (0.5% w/v) and stirred at 150 rpm for 4 h at a constant temperature of 50 °C, followed by ultrasonication for 15 min (Elmasonic E 70H Ultrasonic 37 kHz and 120 W output, Germany). The modification was carried out with a CNC:CTAC ratio of 1:2. Following mixing at 50 °C for 4 h, the mixing was continued at 30 °C overnight to ensure a homogenous attachment of CTAC onto CNC and its completion. Next, modified CNCs were subjected to centrifugation (6000 rpm) for 3 cycles of 20 min each to eliminate unbound CTAC and excess NaOH. Herein, modified CNC with CTAC was denoted as CTAC-CNC.

Calcium phosphate (denoted as CaP) was prepared using 0.05 M $CaCl_2$ and 0.05 M sodium monohydrogen phosphate (Na_2HPO_4) solutions, to be incorporated with sodium alginate (ALG) and CNC in producing hydrogel beads with a porous structure. The Na_2HPO_4 solution (25 mL) was added dropwise via a 23G Terumo syringe to produce calcium phosphate suspension. Porous CTAC-CNC/ALG@HB were prepared by an ionotropic gelation method employing Ca^{2+} ions. Initially, varying dispersions of CNC-ALG were prepared by dissolving different amounts of sodium alginate in 50 mL of distilled water under magnetic stirring at 40 °C for 1 h, into which different amounts of CTAC-CNC were added to produce a viscous solution. To obtain a homogenous mixture, the suspension was subjected to agitation at a high velocity for 2 h. Next, the homodisperse solution was added with 10 mL of the CaP suspension, and the vigorous agitation was continued for a further 2 h. Then, the uniform formulation obtained was dropped into a $CaCl_2$ solution (5%, w/v) under constant magnetic stirring using different gauge size Terumo syringe needles to produce CaP incorporated hydrogel spheres of varying bead size. The beads were allowed to crosslink in $CaCl_2$ solution and was washed thoroughly with a copious amount of distilled water. Finally, a pH 2 solution was prepared using 0.1 M HCl, and the solidified beads were immersed in the acidic solution under constant stirring for 1 h, causing the disintegration of CaP within the beads.

Structural Characterization of Porous CTAC-CNC/ALG@HB

Functional groups were investigated on an Attenuated Total Reflectance-Fourier Transform Infrared (ATR-FTIR) spectrometer (FT-NIR Frontier, PerkinElmer, Germany). Scanning Electron Microscope (FEI Quanta 650 FEG SEM, Holland) was employed to establish freeze-dried hydrogel beads' cross-section morphology, elemental composition and porous structure. X-ray Photoelectron Spectroscopy (XPS, AXIS Ultra DLD, Kratos, UK) wide scan spectra were acquired to infer the adsorption mechanism by analyzing the electron binding energies of the elements before and after adsorption. Brunauer–Emmett–Teller (BET) analysis was conducted on a Micromeritics ASAP 2020 adsorption analyzer (USA, Version 4.04) to deduce the pore size distribution and the specific surface areas of the beads. The pH point zero charge (pH_{pzc}) was ascertained by the pH drift method. The surface charges were assessed on a zeta potential tester (Zetasizer Nano-ZS, Malvern Instruments, UK). The thermal degradation behaviour of the beads was examined on a thermal gravimetric analyzer (STA 6000, PerkinElmer, UK). E-supplementary material (Text S7 and Fig. S1) details the optimization of hydrogel beads.

Water content, swelling behaviour (% ratio) and porosity of CTAC-CNC/ALG and pure ALG hydrogel beads were determined through the gravimetric method. Water content was ascertained by drying the beads at 40 °C until a constant weight was obtained. To deduce the degree of swelling, a specific amount of freeze-dried beads were added into ultrapure water at 30 °C and left for 24 h. The water absorbency (%) was determined based on Eq. (1) [22]:

$$Degree\ of\ swelling\ (\%) = \left(\frac{W_w - W_d}{W_d}\right) \times 100 \quad (1)$$

where W_w refers to the wet weight (g) of the swollen hydrogel beads upon swelling and W_d is the weight of the freeze-dried hydrogel beads (g).

Porosity was determined attributed to the density of pure ALG bead matrix and modified CNC-ALG bead matrix, and

the weight difference before and after drying. Equation (2) describes the calculation of porosity of hydrogel beads [3]:

$$Porosity\ (\epsilon) = \left(\frac{\left(\frac{W_w - W_d}{\rho_w} \right)}{\left(\frac{W_d}{\rho_m} \right) + \left(\frac{W_w - W_d}{\rho_w} \right)} \right) \quad (2)$$

where ρ_w and ρ_m are the densities of water and bead matrices, respectively.

Adsorption Performance

A series of adsorption studies were performed using the batch equilibration method in triplicate, and the average values were reported for each data analysis. The initial and residual concentrations of 4-chlorophenol were quantified on a Shimadzu UV-2600 UV–Vis spectrophotometer (Japan). % 4-chlorophenol uptake and the equilibrium adsorption capacity of hydrogel beads were evaluated according to the following equations:

$$Percentage\ 4-chlorophenol\ removal = \frac{(C_0 - C_e)}{C_0} \times 100 \quad (3)$$

where C_o refers to the initial 4-chlorophenol concentration (mg L^{-1}) and C_e is the equilibrium concentration (mg L^{-1}) of free 4-chlorophenol molecules in the solution.

$$q_e = \frac{(C_0 - C_e)V}{m} \quad (4)$$

where q_e is the adsorption capacity of hydrogel beads (mg g^{-1}) at equilibrium, V is the volume (L) of 4-chlorophenol solution, and m is the dosage of fabricated hydrogel beads in grams.

Influence of Various Parameters on 4-Chlorophenol Adsorption

Various conditions could affect the adsorptive removal of 4-chlorophenol by porous CTAC-CNC/ALG@HB. Therefore, the effects of crosslinking time, hydrogel bead size, adsorbent dosage, initial 4-chlorophenol concentration, medium pH, shaking speed, contact time and temperature were assessed, governing the adsorption capability of hydrogel beads.

Adsorption Isotherms

Adsorption isotherm studies of porous CTAC-CNC/ALG@HB were conducted by subjecting 1.0 g of hydrogel beads under constant shaking at 250 rpm for 6 h at pH 4 with various initial 4-chlorophenol concentrations (100, 200, 400, 600 and 800 mg L^{-1}) and temperatures (30, 40 and 50 °C). The beads' equilibrium adsorption capacity (q_e) was then plotted against the equilibrium concentration of 4-chlorophenol (C_e) and modelled by applying Langmuir, Freundlich, Temkin and Dubinin-Radushkevich mathematical models to determine the interactive behaviour between the beads and the 4-chlorophenol through adsorption isotherms.

Adsorption Kinetics

In order to investigate the kinetics of the adsorption process, the samples were withdrawn at predetermined time intervals (0 to 180 min) to analyze the 4-chlorophenol concentration in the solution until attaining the adsorption equilibrium. 1.0 g of porous CTAC-CNC/ALG@HB of seven different batches (50, 100, 200, 400, 600, 800 and 1000 mg L^{-1}) was agitated at 30 °C, pH 4 and 300 rpm. The adsorption capacity at contact time t (q_t, mg g^{-1}) was plotted against time (t) to infer the time evolution of adsorption. The experimental data were tailored with the pseudo-first-order, pseudo-second-order (type 1), Elovich and intraparticle diffusion models. q_t values were computed according to Eq. (5);

$$q_t = \frac{(C_0 - C_t)V}{m} \quad (5)$$

where C_o, m and V have their usual meanings as stated above. C_t refers to the concentration (mg L^{-1}) of 4-chlorophenol at contact time t.

Applicability of Adsorption Isotherms and Kinetic Models

The validity of the isotherm and kinetic models were justified by evaluating the adjusted correlation coefficient (Adj. R^2), the root mean square error (RMSE), reduced Chi-square (χ^2) estimation and the residual sum of squares (RSS) statistical parameters concerning the experimental data and the model estimates, which were applied to evaluate the adsorption behaviour of 4-chlorophenol. The details regarding these equations have been stated in E-supplementary material.

Reusability Study

After 4-chlorophenol adsorption (initial 4-chlorophenol concentration: 100 mg L^{-1}, dosage: 1 g, contact time: 6 h), the exhausted hydrogel beads were withdrawn by simple filtration and then thoroughly washed with ultrapure water. Next, the beads were submerged in 100 mL of 99% ethanol (eluent) and shaken for 5 h at ambient room temperature to restore the adsorption sites of hydrogel beads. Finally, the hydrogel beads were immersed in 100 mL of 5 wt% $CaCl_2$ solution to undergo solidification for 6 h and washed

with ultrapure water. Simultaneously, the concentrations of 4-chlorophenol in the solution were detected by UV–Vis spectrometry at 280 nm.

Results and Discussion

Characterization of Porous CTAC-CNC/ALG Hydrogel Beads

CTAC-CNC/ALG beads recorded an average swelling ratio of 155%, while pure ALG beads achieved an average swelling ratio of 205%. According to Mohammed et al. [3], the addition of CNCs into the ALG polymer matrix enhances its crystallinity, hence attaining a lower swelling ratio than pure ALG hydrogel beads. Some previous studies [3, 12, 23, 24] have demonstrated that CNC as a filler could reinforce hydrogel beads, resulting in increased mechanical properties. Figure 1 illustrates a comparison of water content, porosity and swelling ratio of CTAC-CNC/ALG and pure ALG hydrogel beads. The incorporation of CNCs into the ALG polymer matrix does not impart a significant impact on the water content and porosity of hydrogel beads. However, since the addition of CNCs into the ALG polymer matrix enhanced its adsorption capability without compromising its porosity, it can be suggested that CNCs contributed to enhancing the number of adsorption sites owing to its higher BET surface area (24.99 m^2 g^{-1}). Thus, increased 4-CP adsorption characteristics were achieved in comparison to pristine ALG hydrogel beads.

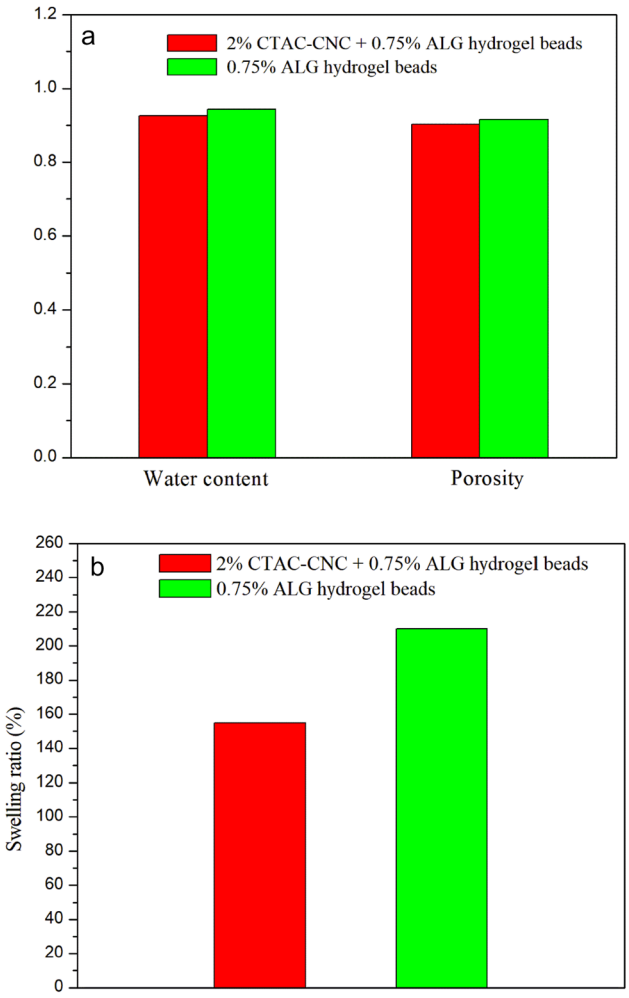

Fig. 1 **a** Comparison of water content and porosity of CTAC-CNC/ALG and pure ALG hydrogel beads, and **b** swelling ratio of CTAC-CNC/ALG and pure ALG hydrogel beads

FTIR Spectroscopy

FTIR analysis can identify the chemical functional groups of biopolymers such as nanocellulose-based hydrogel beads and establish their molecular interactions. This analysis assessed the surface chemistry of pure calcium alginate (ALG) hydrogel beads and CTAC-CNC/ALG hydrogel beads. Initially, the modification of CNC was validated by studying the chemical functionalities of pristine CNC and CTAC-modified CNC. According to Fig. 2a, unmodified CNC (red line) and CTAC-CNC (blue line) exhibited similar peaks positioned at 3334, 2894, 1594, and 893 cm^{-1}, corresponding to stretching vibrations of –OH, aliphatic saturated C–H stretching, O–H bending vibrations of adsorbed water and β-glycosidic linkages (C-H rocking vibration) of cellulose, respectively which are characteristic signals for CNC obtained from oil palm fronds [25]. The appearance of vibrational bands of 3334, 1097, and 893 cm^{-1} in pristine and CTAC-modified CNC substantiated that CNCs were made up of cellulose type I polymorph [17]. In addition, the highest intensity peak located around 1000 cm^{-1} denotes the pyranose ring ether band of cellulose [26]. The FTIR spectrum of CTAC-CNC showed symmetric and asymmetric $–CH_2$ stretching vibrations of the long alkyl chain of CTAC at 2850 cm^{-1} and 2920 cm^{-1}, respectively. Furthermore, a new peak was observed at 1467 cm^{-1}, indicating the trimethyl groups of quaternary ammoniums [17, 26, 27]. The black line in Fig. 2a signifies CTAC data. The absence of these signals in the IR spectrum obtained for CNC suggests the successful grafting of CTAC into CNC. The presence of sulfate groups in CNC consequent to sulfuric acid hydrolysis was specified by the IR peak centered at 1167 cm^{-1} [28].

Figure 2b shows the FTIR spectra of sodium alginate powder (SA) and pure ALG beads along with CTAC-CNC/ALG hydrogel beads. The absorption bands of SA (black line) pertained at 3269 (broad band), 2918, 1597, 1408, and 1024 cm^{-1} were consistent with -OH stretching vibration, C–H stretching, asymmetric and symmetric C=O stretching vibrations of $–COO^-$ group, and C–O–C stretching, respectively [29, 30]. However, it is interesting to note that there

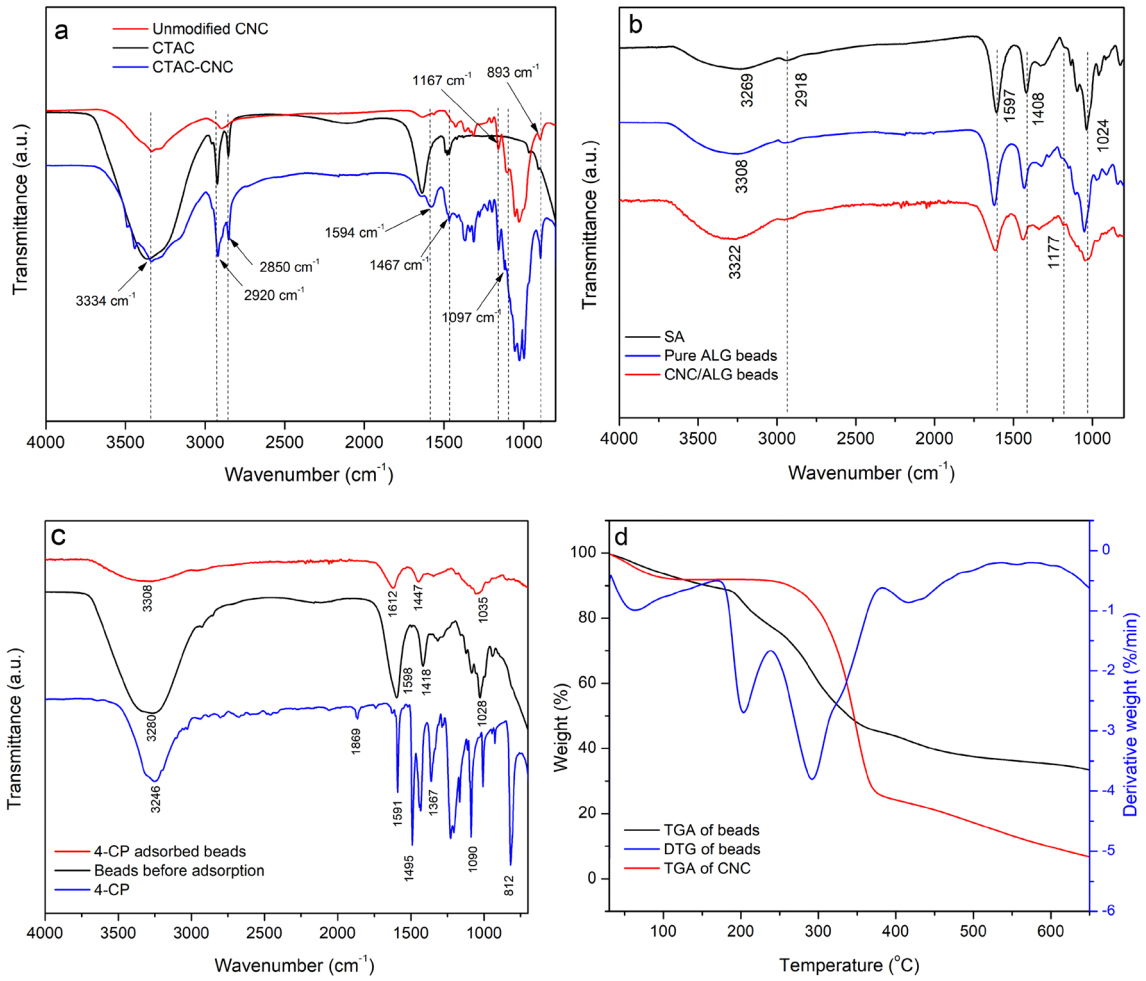

Fig. 2 FT-IR spectra of **a** unmodified CNC, CTAC and CTAC-CNC, **b** SA, pure ALG and CNC/ALG beads, **c** beads before adsorption and 4-CP loaded beads, and **d** TGA and DTG plots of beads

were noticeable shifts in asymmetric and symmetric stretching vibrations of $–COO^-$ bands to 1610 and 1428 cm^{-1}, respectively, in the IR spectrum acquired for pure ALG beads compared to SA. The transition of these signals to higher wavenumbers could owe to the establishment of ionic bonding (crosslinking) between $–COO^-$ groups of sodium alginate and Ca^{2+} ions [31]. Upon closely analyzing the peaks obtained for CNC/ALG hydrogel beads, it is evident that the IR band analogous to –OH stretching was slightly more intensified and broader than the peaks of SA, owing to the presence of higher content of OH groups in CNC. Meanwhile, the intensity of peaks representing $–COO^-$ stretching reduced with CNC incorporation. It is also evident that the C–H stretching vibration peak in the range of 2800–3000 cm^{-1} was much less prominent in the spectrum representing CNC/ALG hydrogel bead due to the crosslinking reaction [30]. The peak located at 1177 cm^{-1} characterizes the sulfate groups present in CNC.

Figure 2c was acquired to investigate the interaction between the fabricated hydrogel beads and 4-chlorophenol, which depicts IR bands of hydrogel beads before and after 4-CP adsorption. It is worth noting that the IR spectrum of CTAC-CNC/ALG hydrogel beads comprises all the characteristic peaks corresponding to the functional groups of CNC and ALG, which suggests its structural integrity. The FTIR spectrum of 4-CP demonstrates characteristic peaks attributed to C=C stretching at 1591 and 1495 cm^{-1}, in-plane C–H bending vibration at 1367 cm^{-1}, C–Cl stretching vibration (1090 cm^{-1}) and out-of-plane C–H vibration of the aromatic ring at 812 cm^{-1} [32, 33]. Concerning fabricated beads before adsorption, 4-CP loaded beads showed fewer peaks, and there were noticeable shifts in peak positions to higher wavenumbers. In addition, the absorption bands were weakened after adsorption, which highlighted that functional groups of hydrogel bead adsorbent participated in binding 4-CP molecules.

Thermal Behaviour

The thermogravimetric analysis evaluated the thermal stability of fabricated hydrogel beads, as shown in Fig. 2d. The thermal behaviour of CTAC-CNC/ALG@HB demonstrates a four-stage weight loss during the degradation process. The initial stage of the removal of chemisorbed and physically adsorbed water in the hydrogel bead matrix [34] represented a 10.33% mass loss in the temperature region of 78 to 194 °C. The second and third stages corresponded to a sharp reduction of weight, owing to the preliminary degradation of the alginate matrix [35, 36] (DTG_{max} = 203 °C) with a weight loss of 12.03% and preliminary degradation of CNC (DTG_{max} = 294 °C) [12], respectively. The weight loss of CNC is attributed to 44.98%, which signifies the high CNC:ALG ratio of the fabricated beads. The red line characterises the TGA of pristine CNC consisting of a maximum degradation temperature (DTG_{max}) of 338 °C [37, 38]. Interestingly, DTG_{max} of the third stage related to the decomposition of CNCs was lower than that of pure CNC, which may probably be due to the partial degradation at first with subsequent further degradation. The final stage of weight loss (20.59%) occurred between 356 and 477 °C (DTG_{max} = 426 °C) could be due to the further degradation of remaining chemical moieties of hydrogel beads [39], upholding its good thermal properties for 4-CP remediation to withstand moderately high working temperature range up to 194 °C.

Textural Characterization

Textural characterization of porous CTAC-CNC/ALG@HB was investigated employing BET and scanning electron microscopy (SEM) analyses. Scanning electron microscopy analysis is a fundamental tool that has been frequently employed to characterize the surface morphology and underlying physical properties of an adsorbent by inspecting the respective microscopic images. Figure 3 depicts the surface profile features of pure alginate hydrogel beads and their cross-section (a–b), scanning electron micrographs of porous CTAC-CNC/ALG@HB and their cross-section before adsorption (c–d) and after adsorption (e–f). According to Fig. 3c and e, porous CTAC-CNC/ALG@HB surfaces did not alter considerably (no damage upon adsorption) during the adsorption process, indicating that CTAC-CNC/ALG@HB possessed good mechanical properties. Moreover, CTAC-CNC/ALG@HB possess a significantly high number of pores than pure alginate beads, allowing more 4-CP molecules to be adsorbed into these pores and microstructures. Hence, the rough surface structure of CTAC-CNC/ALG@HB was able to produce more humps to enhance the surface area and consequently offer more adsorption sites.

BET analysis (Table 1) for porous CTAC-CNC/ALG@HB also affirmed the porous nature of the fabricated hydrogel beads, reporting a relatively high BET specific surface area of 60.56 $m^2\ g^{-1}$, single point adsorption total pore volume of 0.0144 $cm^3\ g^{-1}$ and total adsorption average pore width of 13.57 nm. BET surface area of pure ALG beads acquired in this study was comparable to that of pristine sodium alginate hydrogel beads reported by Ren and coworkers [30]. The incorporation of calcium phosphate (CaP) into the hydrogel beads and its disintegration within the beads using 0.1 M HCl was able to produce a mesoporous adsorbent since CTAC-CNC/alginate hydrogel beads attained a total adsorption average pore width of 13.57 nm, corroborating a mesoporous pore network (2–50 nm) [40].

According to the IUPAC classification, the adsorption isotherm of 4-CP on porous CTAC-CNC/ALG@HB is of type IV (Fig. S2). The measured BET surface area of the prepared hydrogel beads was comparable to cellulose-based beads reported in the literature that is, modified activated carbon/magnetic cellulose-based beads [41] (90.05 $m^2\ g^{-1}$), polyethyleneimine-grafted porous cellulose beads [42] (100.61 $m^2\ g^{-1}$), cellulose nanocrystals-activated carbon hydrogel beads [43] (85.19 $m^2\ g^{-1}$), porous cellulose hydrogel beads [44] (36.5 $m^2\ g^{-1}$), glutaric anhydride-grafted porous microcrystalline cellulose beads [45] (18.51 $m^2\ g^{-1}$), hollow polyethyleneimine-grafted carboxymethyl cellulose beads [46] (14.889 $m^2\ g^{-1}$) and porous cellulose nanofiber-alginate hydrogel beads [47] (11.694 $m^2\ g^{-1}$).

Determination of Point of Zero Charge (pH_{PZC}) and Zeta Potential

The point of zero charge, in general, is described as the pH at which the net charge of the total adsorbent surface is equal to zero. The zero surface charge characteristics (the isoelectric point) of CTAC-CNC/alginate hydrogel beads were ascertained through the pH drift method, also known as the solid addition method reported elsewhere [48]. The point of intersection of the ΔpH ($pH_{intial} - pH_{final}$) versus $pH_{initial}$ curve with abscissa, at which ΔpH is zero (where $pH_i = pH_f$), is ascribed as pH_{PZC} of the adsorbent. The pH_{PZC} of CTAC-CNC/alginate hydrogel beads was 6.76 (Fig. S3a), which indicates that the net charge of the total hydrogel bead surface is positively charged at pH below 6.76. In contrast, the hydrogel bead surface possesses negative charges at pH values higher than 6.76.

The zeta potential of CNC/ALG@HB and CTAC-CNC/ALG@HB (Figure S3b) were determined under neutral pH conditions. It was evident that surface functionalization through cationic CTAC surfactant significantly enhanced the hydrophobic nature of the hydrogel beads. CNC/ALG@HB acquired a zeta potential of − 18.4 mV, while CTAC-CNC/ALG@HB attained a zeta potential of

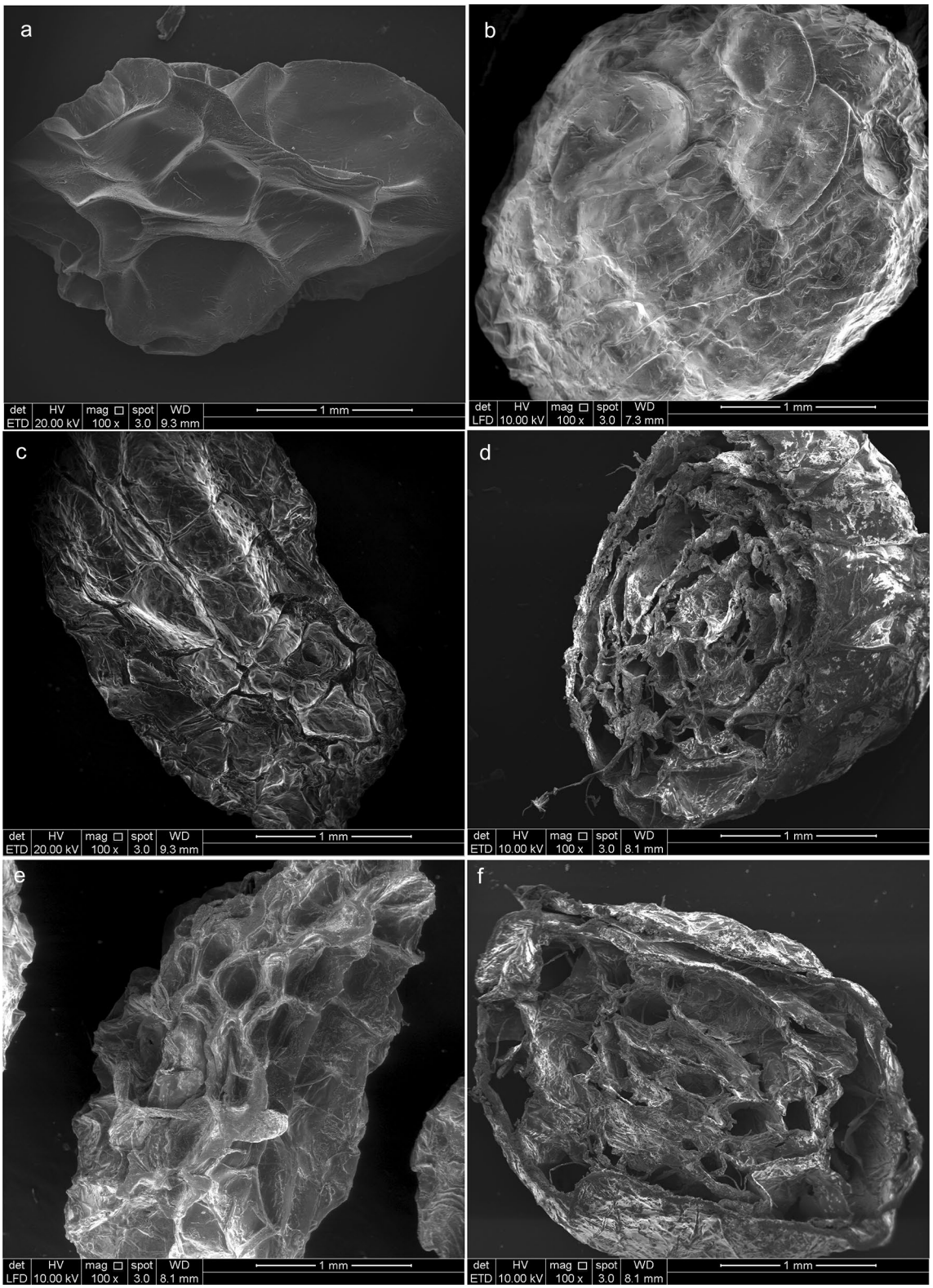

Fig. 3 Surface morphology of pure alginate hydrogel beads and its cross-section (**a**, **b**), surface morphology of porous CTAC-CNC/alginate hydrogel beads and its cross-section before adsorption (**c**, **d**) and after adsorption (**e**, **f**)

Table 1 Specific surface area and porosity characteristics of CNC, pure alginate hydrogel beads, and CTAC-CNC/alginate hydrogel beads

Sample	BET specific surface area ($m^2\ g^{-1}$)	Single point adsorption total pore volume ($cm^3\ g^{-1}$)	Total adsorption average pore width (nm)
Cellulose nanocrystals (CNC)	24.99	0.0084	4.178
Pure alginate (ALG) hydrogel beads	0.386	0.0011	2.187
Porous CTAC-CNC/ALG hydrogel beads	60.56	0.0144	13.57

− 0.603 mV. The slight negative zeta potential obtained at pH 7 could be since the pH_{pzc} of CTAC-CNC/ALG@HB was ascertained to be 6.76. A medium pH higher than its pH_{pzc} would alter the surface charges of the hydrogel bead surface to possess an overall negative charge. Thus, zeta potential data is helpful in further justifying the results obtained through FTIR and XPS analyses.

Influence of Various Parameters on 4-Chlorophenol Adsorption

Chemical and physical experimental conditions could affect the equilibrium adsorption of organic contaminants. In order to elucidate the efficiency of 4-CP adsorption by CTAC-CNC/ALG@HB, the influence of various experimental factors/conditions were examined, which are explained in detail as stated below. With regards to the interference of different pollutants, the presence of co-existing anionic contaminants could depress the adsorption capacity of CNC-based hydrogel beads. As reported by previous studies [49, 50], the use of trimethylammonium cationic surfactants such as CTAC in the modification of adsorbents has shown preferential adsorption towards anionic contaminants, including perchlorate, nitrate, chromate, and sulphate. However, it is important to note that adsorbents' and pollutants' charge characteristics, molecular arrangement and their size influences the selectivity of an adsorbent, hence its adsorption efficiency. Shen [51] reported that phenolic contaminants demonstrate preferential adsorption towards trimethylammonium cationic surfactants-modified adsorbents. Fan and co-workers [49] in their study noted that at low concentration, the influence of other co-existing anions in occupying adsorption sites of CTAC-modified activated carbon was not significant. Mangrulkar et al. [52] reported that the effect of interference of ions on the removal efficacy of chlorophenols is less pronounced as compared to phenol removal due to chlorophenols less tendency to ionize to form phenolate ions. Since low concentration wastewater treatment is one of the major applications of the developed adsorbent in the present study, the interference of co-existing anions was not examined.

Effect of Contact Time and Optimum Dosage

The effect of contact time on 4-CP removal efficiency was investigated for an initial 4-CP concentration of 100 mg L^{-1} employing a fixed amount of hydrogel beads at 30 °C and neutral solution pH. The kinetics of 4-CP adsorption on hydrogel beads were assessed over an adsorption time of 15 min to 24 h. According to the results presented in Fig. 4a, it can be noticed that there was a rapid 4-CP uptake initially with a subsequent slower removal rate until an equilibrium state was attained. The initial fast kinetics at a lower contact time (within the first hour), which showed approximately 60% adsorption, can be associated with the availability of an ample amount of vacant active sites (functional groups) on the surface of hydrogel beads, allowing more 4-CP molecules to get adsorbed. With time-lapse, 4-CP molecules that occupied the adsorption sites impart repulsive forces towards 4-CP molecules in the bulk phase [53] and ultimately, upon saturation of the adsorbent, a plateau is reached. This trend tallies with the data obtained by Heydaripour et al. [53] and Hameed et al. [54] for the adsorption of 4-chlorophenol on porous magnetic resin-g-chitosan beads and rattan sawdust-derived activated carbon, respectively. Based on the binding isotherm depicted in Fig. 4a, the optimal contact time to reach an equilibrium state of adsorption was around 3 h. Thus, all successive adsorption studies were carried out for an adsorption period of 3 h.

The effect of the amount of CTAC-CNC/ALG@HB on 4-CP uptake efficiency (% removal) and adsorption capacity (q_e) was assessed by varying the adsorbent dosage in the range of 0.25–5.0 g/100 mL. According to the results presented in Fig. 4c, adsorption efficiency increased distinctly from 50.99 to 73.96% by increasing the hydrogel beads' dosage from 0.25 to 1.0 g. Higher percentage of 4-CP removal was due to the availability of high content of vacant surface-active binding sites, attributing to a higher ratio between adsorption sites to adsorbate [53]. The adsorption capacity reduced sharply from 20.18 to 7.32 mg g^{-1} with the increase in hydrogel bead dose from 0.25 to 1.0 g, owing to the lower ratio between the amount of 4-CP adsorbed to the mass of adsorbent available. This observation trend is coherent with the data reported by Yasir and co-workers [55] and Nadavala et al. [56]. However, the increment in adsorption efficiency

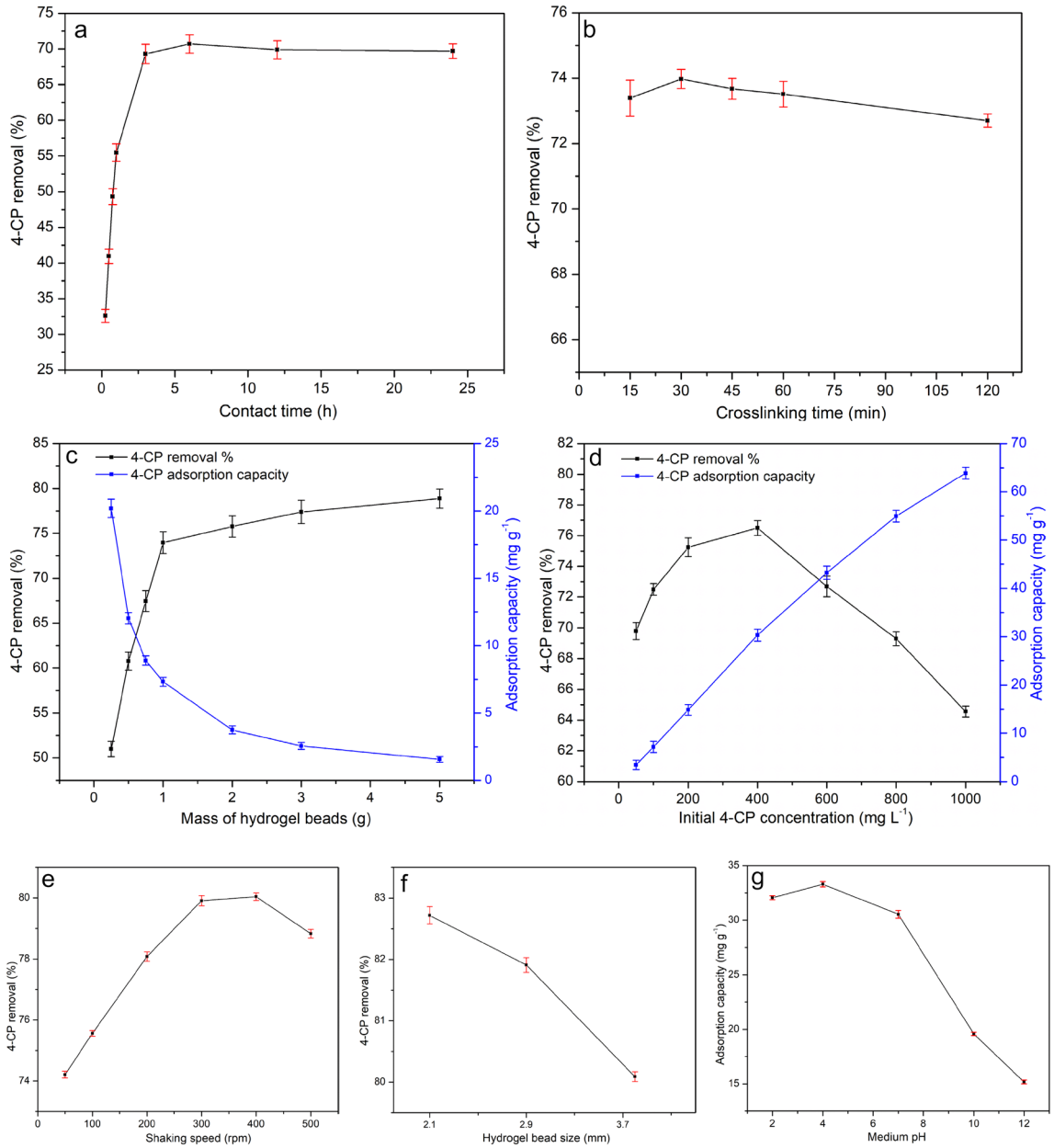

Fig. 4 Influence of **a** contact time, **b** crosslinking time, **c** adsorbent dosage, **d** initial 4-CP concentration, **e** shaking speed, **f** hydrogel bead size and **g** medium pH on the 4-chlorophenol adsorption characteristics by porous CTAC-CNC/ALG hydrogel beads

of 4-CP was insignificant above 1.0 g adsorbent dosage. Moreover, the adsorption capacity obtained with an adsorbent mass above 1.0 g was relatively low. Hence, 1.0 g was determined as the optimum dose of hydrogel beads in terms of the efficiency of 4-CP uptake and adsorption capacity.

Effect of Initial 4-Chlorophenol Concentration

The influence of the initial concentration of 4-CP adsorbate on its removal efficiency was investigated by employing seven different batches of initial concentrations in the range of 50–1000 mg L^{-1} for a fixed amount of hydrogel beads and adsorption time at 30 °C under neutral solution pH. According to Fig. 4d, the removal efficiency increased up to an initial adsorbate concentration of 400 mg L^{-1}, and after that, with an increased 4-CP concentration above 400 mg L^{-1}, the removal % decreased progressively. The initial increment in 4-CP removal efficiency could be related to the lower ratio between the amount of 4-CP molecules available to the number of adsorption sites. Once the initial 4-CP concentration was increased above the optimum concentration, the increment in the number of 4-CP molecules that approach

the adsorbent surface exceeds the number of adsorption sites available per 4-CP molecule, resulting in a reduced 4-CP removal uptake. Although the efficiency of 4-CP uptake was reduced with increased adsorbate concentration, the adsorption capacity increased from 3.455 to 63.882 mg g^{-1} for initial 4-CP concentrations of 50 mg L^{-1} and 1000 mg L^{-1}, respectively. The increased adsorption capacity corresponds to the transfer of more 4-CP molecules to the hydrogel bead surface from the bulk solution. As a result, the availability of more 4-CP molecules with increased initial 4-CP concentration contributed to a greater driving force (higher flux) for mass transfer (diffusion) to occur from the bulk phase to the surface active sites [55].

Effect of Medium pH

In this study, the modification of CNCs with CTAC cationic surfactant transformed CNCs to be hydrophobic [17], which was also affirmed through FTIR analysis. Mohammed et al. [3] reported that the pH of the medium contributes immensely to tailoring the surface charge of CNC/alginate-based hydrogel beads through the protonation or deprotonation of its functional groups. In this work, functional groups, including trimethyl groups [$(CH_3)_3N^+$] of the quaternary ammonium salt, carboxyl (–COOH), hydroxyl (OH) and sulfate ($–OSO_3^-$) of the fabricated beads can participate as chelating sites to bind with 4-CP. According to Fig. 4g, the adsorption capacity of hydrogel beads towards 4-CP demonstrated an increment with increasing initial solution pH of 4-CP solution from 2 to 4. Even though, increasing the pH up to 7 slightly reduced the adsorption performance, it still exhibited a favourable adsorption in terms of the adsorption capacity, but further increase in solution pH above 7 hindered the adsorption capability of the hydrogel beads.

At a specific medium pH, 50% of their molecules get converted to their anionic form at $pH = pK_a$ of chlorophenols [54]. Hence, 4-chlorophenol undergoes ionization (deprotonation) and becomes negatively charged in solutions with pH values higher than its pK_a ($pH > pK_a$) or near to its pK_a value. The pK_a value corresponding to 4-chlorophenol is 9.41 [57]. Therefore, a negatively charged 4-CP ion (phenoxide) is much less hydrophobic in a medium pH greater than 9 ($pH > 9$) and the concentration of phenoxide ions increases with increasing background pH. Therefore, repulsive forces would impede 4-CP adsorption under basic conditions as a result of deprotonation of the –OH and –COOH groups of CTAC-CNC/ALG@HB, hence the adsorbent carried an overall negative charge. On the other hand, 4-chlorphenol would exist in its non-ionized form (neutral) in media with pH values below 9 ($pH < 9$) [54]. The undissociated form of 4-CP should contribute to a higher 4-CP removal efficiency below pH 9 if the adsorbent possess a hydrophobic surface. However, the isoelectric point of CTAC-CNC/ALG@HB is 6.76, which means that the adsorbent is positively charged only at solution pH values below 6.76. Based on this study, it can be suggested that CTAC-CNC/ALG@HB is effective as a potential adsorbent in the pH range below neutral pH.

Adsorption Isotherm Modelling

Adsorption isotherm modelling is one of the widespread approaches to assessing the adsorption performance of an adsorbent. Adsorption isotherms are mathematical expressions that explain adsorbate diffusion from the solution phase to the solid phase (adsorbent phase) at equilibrium. More importantly, equilibrium studies of adsorption provide information on the feasibility of eliminating an adsorbate and determining the affinity and surface properties of the adsorbent [35, 43]. According to the Langmuir isotherm, no further adsorption could occur once the surface active sites have encountered adsorption.

A higher Adj. R^2 value and lower values of χ^2, RMSE and RSS would generally indicate a good fit between experimental and calculated data [58, 59]. Table 2 summarizes the calculated parameters q_m, K_L, K_F, n and other adsorption parameters pertaining to Temkin and Dubinin–Radushkevich isotherms calculated from the slope and intercept of corresponding plots. The symbols in Fig. 5 denote experimental data, while curves and regression plots correspond to simulated data (n = 3). According to Fig. 5 and Table 2, it is evident that Langmuir (type 1) adsorption isotherm best described the adsorption of 4-chlorophenol onto CTAC-CNC/ALG@HB throughout the researched solution temperature range (30–50 °C) achieving the highest goodness of the fit. Additionally, the linearized forms of Langmuir and Freundlich isotherms attained better correlation with the equilibrium data compared to their non-linear counterparts (Table S1). The adsorption isotherm models fitted the experimental data in the order of Langmuir-type (I) > Freundlich > Temkin > Dubinin–Radushkevich isotherm. The Linearized Langmuir type 1 model offered the highest linear regression fitting coefficient (Adj. R^2) in the range of 0.9974–0.9985, and the lowest χ^2, RMSE and RSS values are shown in Table 2. Thus, the goodness of the fit towards the Langmuir isotherm implies that the hydrogel bead surface consists of homogenous surface active sites [35], and 4-CP adsorption occurred in the manner of a monolayer. The maximum adsorption capacity (q_m) achieved was 64.935 mg g^{-1} at 30 °C.

The R_L values obtained were in the range of 0.1352–0.5924 (Table S2), affirming that the 4-CP adsorption process proceeded favourably. According to the linear Freundlich isotherm, the n value was 1.6236 at 30 °C and 1.8253 at 50 °C, further indicating favourable 4-CP adsorption. Heydaripour and coworkers [53] reported that 4-chlorophenol adsorption onto magnetic porous

Table 2 Isotherm model parameters calculated using the linear regression method for 4-chlorophenol adsorption from wastewater

Isotherm model	Non-linear			Linear		
	303.15 K	313.15 K	323.15 K	303.15 K	313.15 K	323.15 K
Langmuir						
q_m (mg g^{-1})	65.709	52.183	47.081	64.935	52.632	46.685
K_L (L mg^{-1})	0.0683	0.0745	0.0781	0.0707	0.0768	0.0799
Adjusted R^2	0.9995	0.9986	0.9984	0.9981	0.9974	0.9985
RMSE	0.3412	0.4948	0.2382	0.0870	0.1561	0.1405
χ^2	0.1164	0.2449	0.4881	0.0075	0.0243	0.0197
RSS	0.3493	0.7347	0.7147	0.0227	0.0731	0.0593
Freundlich						
K_F [(mg g^{-1}) (L $g^{-1})^{1/n}$]	2.0822	2.1275	2.2411	1.4023	1.5065	1.4585
n	1.8594	1.7898	2.1436	1.6236	1.7896	1.8253
Adj. R^2	0.9775	0.9782	0.9567	0.9827	0.9813	0.9686
RMSE	2.3562	1.9366	2.5079	0.4107	0.3970	0.5022
χ^2	5.5518	3.7506	6.2897	0.0169	0.0158	0.0252
RSS	16.655	11.251	18.869	0.0506	0.0473	0.0757
Temkin						
B_T				13.445	10.965	10.195
K_T (L g^{-1})				0.0819	0.0833	0.0812
ΔH_T (J mol^{-1})				187.46	237.43	263.52
Adj. R^2				0.9813	0.9872	0.9896
RMSE				2.1492	1.4809	1.2242
χ^2				4.6192	2.1931	1.4987
RSS				13.857	6.5794	4.4961
Dubinin–Radushkevich (D–R)						
q_m (mg g^{-1})				32.866	29.074	27.796
β (mol^2 kJ^{-2})				0.0891	0.0979	0.1101
E (kJ mol^{-1})				2.3688	2.2591	2.1305
Adj. R^2				0.7354	0.7411	0.7646
RMSE				0.3701	0.3406	0.3169
χ^2				0.1369	0.1160	0.1004
RSS				0.4109	0.3481	0.3013

resorcinol–melamine–formaldehyde based resin grafted chitosan beads pursued the Langmuir isotherm model. In relation to the Temkin equation, a more considerable K_T value represents a greater inter-adsorbate interaction [54]. However, the present study reported K_T values around 0.08 L g^{-1} throughout the experimented solution temperature range, denoting lower inter-adsorbate interaction between adsorbed 4-CP molecules. Based on the Dubinin–Radushkevich isotherm model, an adsorption process could be classified as physical adsorption if $E < 8$ kJ mol^{-1} and chemical adsorption (chemical ion-exchange) if kJ $mol^{-1} < E < 16$ kJ mol^{-1} [60]. Activation energies less than 20 kJ mol^{-1} are believed to be corresponding to Van der Waals forces and the predominant physical nature of the adsorption process established through the D–R isotherm is consistent with the results obtained through the thermodynamic study.

Effect of Temperature and Thermodynamics

The present study investigated the temperature dependence of 4-CP adsorption in the range of 303–323 K with an interval of 5 K while maintaining the rest of the influential factors constant. According to Fig. 6a, it is evident that the solution temperature imparted an undesirable impact on the adsorptive removal of 4-CP. It was found that the 4-CP removal efficiency decreased from 76.65 to 58.46% upon increasing the temperature from 30 to 50 °C, implying impeded feasibility of 4-CP adsorption at elevated temperatures. Furthermore, Fig. 6a suggested that 4-CP adsorption capacities decreased with rising temperature, indicative of the exothermic nature of the adsorption process. Even though the movement of 4-CP chemical species in the solution accelerates as the solution temperature rises, the adsorption efficiency is reduced due to the high possibility of desorption.

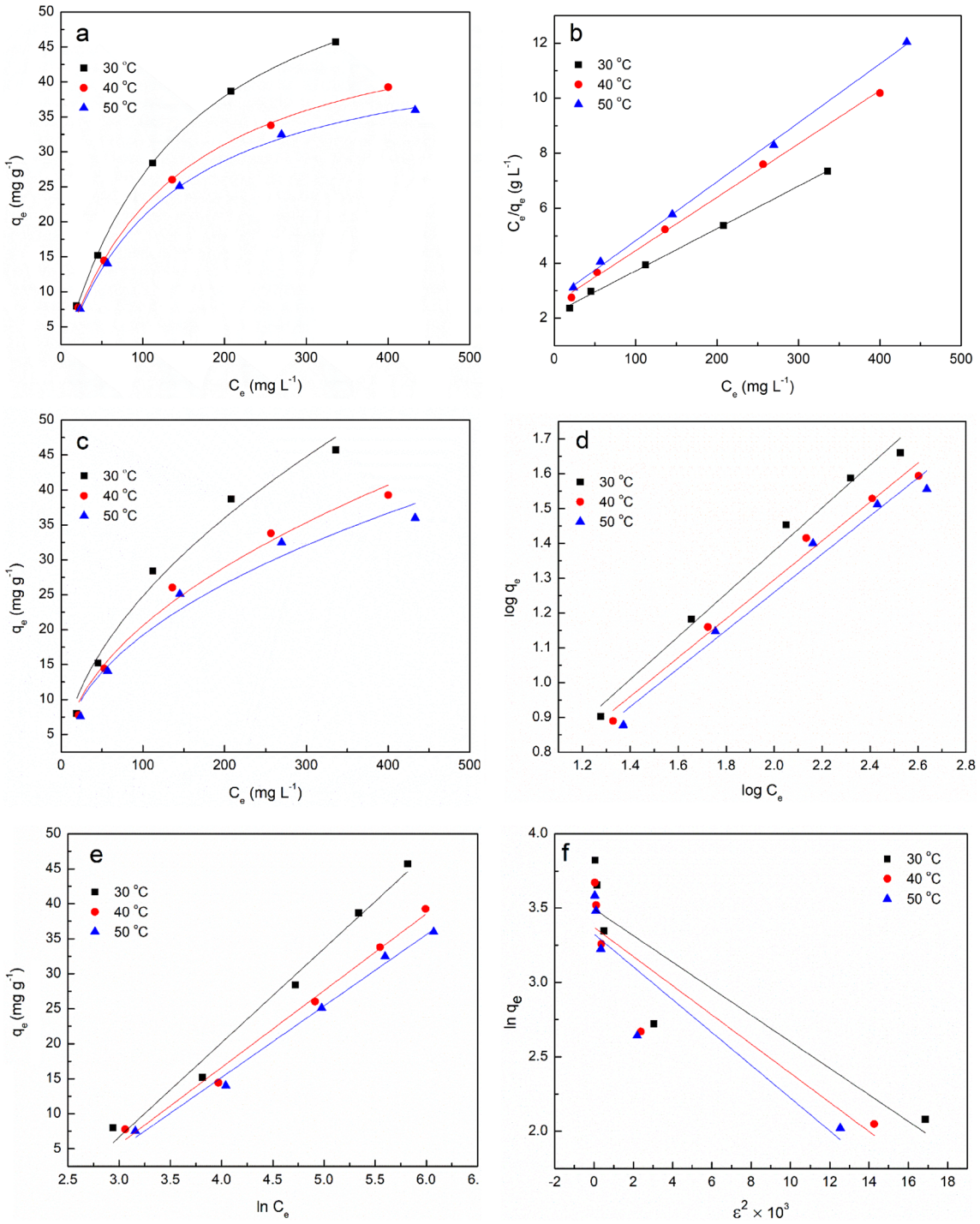

Fig. 5 **a** Non-linear and **b** linear Langmuir isotherm, **c** non-linear and **d** linear Freundlich isotherm, **e** Temkin and **f** Dubinin–Radushkevich isotherm plots representing the adsorption of 4-CP onto CTAC-CNC/ALG hydrogel beads

The reduced adsorptive removal efficiency of 4-CP with increasing solution temperature could owe to two apparent reasons, which are the weakened binding forces between 4-CP molecules and CTAC-CNC/ALG@HB, especially hydrogen bonding and van der Waals interaction, and the destruction of surface-active adsorption sites [3, 61]. Hence, an increased magnitude of adsorption with decreased temperature corroborates a physical adsorption process.

The thermodynamic study allows elucidating the nature of the adsorption process and its spontaneity. Van't Hoff plot (Fig. 6b), which is a plot between ln K_o versus 1/T, can be adopted to infer the thermodynamics of adsorption.

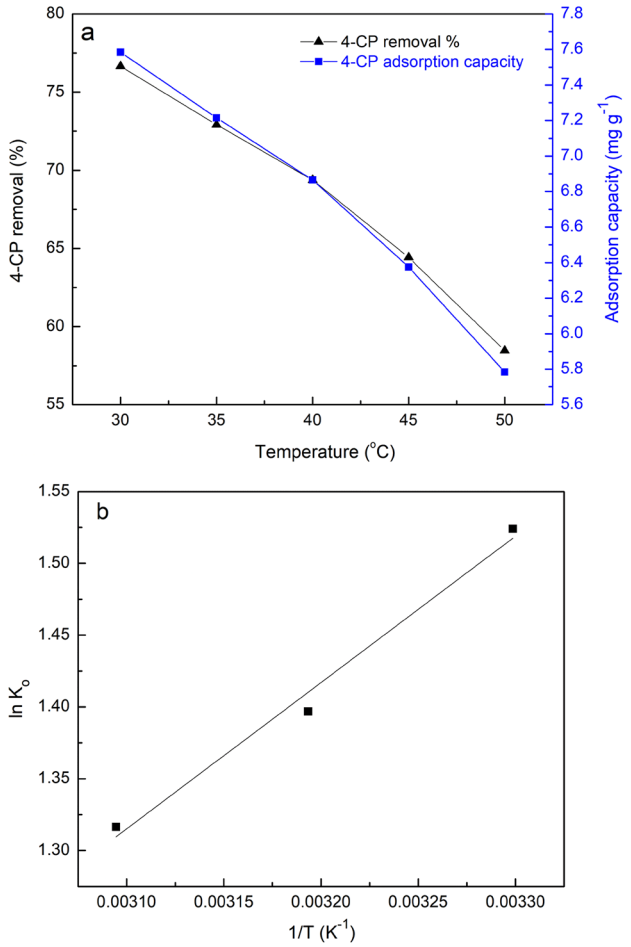

Fig. 6 **a** Effect of temperature on the adsorption of 4-CP onto CTAC-CNC/ALG hydrogel beads (Conditions: pH 7, adsorbent dose 1 g, initial 4-CP concentration 100 mg L^{-1}; contact time 3 h) and **b** van't Hoff plot of ln K_o against 1/T for 4-CP adsorption onto CTAC-CNC/ALG hydrogel beads

The intercept and the slope of the Van't Hoff plot yield the values of standard entropy change (ΔS°) and standard enthalpy change (ΔH°), respectively. Based on the data obtained, ΔH° and ΔS° parameters were estimated to be − 8.473 and − 15.332 J mol^{-1} K^{-1}, respectively. In addition, ΔG° values were determined to be − 3.841, − 3.637, and − 3.536 kJ mol^{-1} at 303.15, 313.15 and 323.15 K, respectively (Table S3). The reduction in the magnitude of ΔG° value with increasing temperature reveals that the spontaneity of the adsorption process is inversely proportional to solution temperature. The negative values obtained for standard Gibbs free energy revealed the thermodynamic spontaneity and feasibility of 4-chlorophenol adsorption onto CTAC-CNC/ALG@HB. ΔH° attained in this study indicated the exothermic nature of the adsorption process, which means that heat evolved upon adsorption. The exothermic behaviour is realized through the negative sign, and its magnitude affirms the occurrence of physical interactions (physisorption) between 4-CP molecules and hydrogel bead surface.

The enthalpy of adsorption attained in this study was negative and lower than 10 kJ mol^{-1} in magnitude, which corresponds to the predominant physical adsorption mechanism of 4-chlorophenol. Thus, obtaining a negative enthalpy for the adsorption process can be correlated to establishing intermolecular forces between the adsorbate and the adsorbent [55, 62]. A smaller negative value obtained for ΔS° revealed that the amount of disorder involved in the adsorption process was comparatively minimum, i.e. decrease in randomness throughout the adsorption process. Heydaripour and co-workers [53] also reported the involvement of a higher degree of the order for 4-CP sorption onto porous magnetic resin-g-chitosan beads. They observed a decreasing trend of 4-CP adsorption with an increase in solution temperature, which implies the adsorption process was exothermic. Madannejad and co-workers [57] observed lower adsorption capacity for 4-CP adsorption onto carbon nanofibers at elevated temperatures, revealing that adsorption proceeded predominantly via physisorption. The physisorption mechanism has been discussed in detail in the latter part of the study.

Adsorption Kinetics

The adsorption kinetic data enlighten the underlying adsorption mechanism through the evaluation of how fast the adsorption process reaches equilibrium. In relation to the kinetic data obtained from the experiment, the pseudo-first-order, pseudo-second-order, Elovich and intraparticle diffusion models were applied to elucidate the mechanism of adsorption and deduce probable rate-controlling steps [63, 64]. Thus, these four linear fitting methods were employed to fit the experimental data to examine the adsorption kinetics. The kinetic parameters of 4-chlorophenol adsorption onto CTAC-CNC/ALG@HB under different initial concentrations were computed and are provided in Table 3. E-supplementary material details the equations used for adsorption kinetic modelling. Plots of q_t versus time for various 4-CP concentrations are depicted in Fig. 7a. Regarding the pseudo-first-order equation, k_1 values for various initial 4-CP concentrations were determined from the slope of the $\ln(q_e - q_t)$ vs time (t) regression plot.

The pseudo-second-order rate (k_2) was evaluated from the intercept of t/q_t vs t (model I) and the slope of $1/q_t$ vs 1/t (model II) regression plots, which are depicted in Fig. 7b. The correlation of the pseudo-first-order and Elovich plots with the experimental kinetic data was poor. The fitting results of the three kinetic models are summarized in Table 3. Based on Table 3, the adjusted correlation coefficient values were in the range of 0.9293–0.9845 for the pseudo-first-order equation, suggesting its unsatisfactory

Table 3 Kinetic constant parameters and determination coefficients calculated using the linear regression method at 30 °C for 4-chlorophenol adsorption from wastewater

Kinetic model	Parameter	4-Chlorophenol concentration (mg L^{-1})						
		50	100	200	400	600	800	1000
Pseudo-first order	k_1 (min^{-1})	0.0328	0.0344	0.0302	0.0319	0.0309	0.0323	0.0534
	$q_{e,cal}$ (mg g^{-1})	1.5914	2.8851	10.398	18.154	20.039	33.452	35.125
	$q_{e,exp}$ (mg g^{-1})	3.5417	8.2934	14.971	25.601	33.593	41.469	48.895
	Adj. R^2	0.9515	0.9293	0.9653	0.9845	0.9763	0.9660	0.9829
	RMSE	0.4191	0.5356	0.3241	0.2268	0.2727	0.3433	0.3983
	χ^2	0.1756	0.2869	0.1050	0.0515	0.0744	0.1179	0.1586
	RSS	1.9322	3.1559	1.1552	0.5660	0.8181	1.2966	1.7452
Pseudo-second order	*Model I*							
	k_2 (g mg^{-1} min^{-1})	0.0488	0.0189	0.0041	0.0023	0.0025	0.0014	0.0037
	k_{2i} (g mg^{-1} min^{-1})	0.6499	1.4182	1.1025	1.8312	3.2278	2.9057	9.3621
	$q_{e,cal}$ (mg g^{-1})	3.6495	8.6625	16.398	28.217	35.932	45.558	50.302
	$q_{e,exp}$ (mg g^{-1})	3.5417	8.2934	14.971	25.601	33.593	41.469	48.895
	Adj. R^2	0.9999	0.9989	0.9983	0.9981	0.9991	0.9984	0.9988
	RMSE	0.1411	0.2161	0.1413	0.0870	0.0464	0.0495	0.0378
	χ^2	0.0199	0.0467	0.0199	0.0076	0.0021	0.0024	0.0014
	RSS	0.2190	0.5137	0.2195	0.0834	0.0236	0.0269	0.0157
	Model II							
	k_2 (g mg^{-1} min^{-1})	0.0644	0.0144	0.0028	0.0017	0.0015	0.0010	0.0025
	$q_{e,cal}$ (mg g^{-1})	3.5323	8.9126	17.794	30.367	39.936	49.044	52.521
	$q_{e,exp}$ (mg g^{-1})	3.5417	8.2934	14.971	25.601	33.593	41.469	48.895
	Adj. R^2	0.9755	0.9702	0.9954	0.9968	0.9888	0.9934	0.9913
	RMSE	0.0107	0.0083	0.0041	0.0019	0.0024	0.0018	0.0007
	χ^2	0.0001	0.0006	0.0002	0.0003	0.0005	0.0003	0.0005
	RSS	0.0013	0.0008	0.0001	0.0004	0.0006	0.0004	0.0006
Elovich	a_e (mg g^{-1} min^{-1})	10.509	6.6094	2.5428	4.2328	9.1091	6.6665	48.657
	b_e (g mg^{-1})	2.2452	0.7454	0.3014	0.1739	0.1501	0.1082	0.1330
	Adj. R^2	0.9451	0.8435	0.9422	0.9447	0.9145	0.9435	0.8531
	RMSE	0.1175	0.6290	0.8987	1.5217	2.2251	2.4759	3.3974
	χ^2	0.0138	0.3957	0.8077	2.3156	4.9509	6.1301	11.542
	RSS	0.1518	4.3527	8.8849	25.472	54.460	67.431	126.964

fit with the adsorption data. However, the pseudo-second-order (model I) equation registered adjusted R^2 values greater than 0.998, implying that the experimental data satisfactorily correlated with the kinetic model. Meanwhile, this model's RMSE, χ^2 and RSS values were lower than the pseudo-first-order and Elovich models. Additionally, the calculated adsorption capacity ($q_{e,cal}$) indicated a close resemblance to the experimental adsorption capacity ($q_{e,exp}$) value, firmly affirming that the sorption of 4-CP by CTAC-CNC/ALG@HB was best explained by pseudo-second-order (model I) kinetics. The adsorption kinetic models fitted the experimental data in the order of pseudo-second-order (model I) > pseudo-second-order (model II) > pseudo-first-order > Elovich model. Kuleyin [65] reported that adsorption kinetics of 4-chlorophenol removal by surfactant-modified zeolite followed the pseudo-second-order (model I) rate equation. Better fit in the pseudo-second-order equation obtained for 4-CP removal suggests a chemisorption process. Madannejad et al. [57] explored the suitability of employing the pseudo-second-order (PSO) kinetic model for the adsorption of 4-CP by carbon nanofibers and found that the model I PSO equation was the best corresponding model with the experimental kinetic data.

Mechanism Analysis of 4-Chlorophenol Adsorption

Intraparticle-Diffusion Model

To gain insights into the adsorption mechanisms and rate-controlling steps influencing adsorption kinetics, the experimental kinetic data were tailored to the intra-particle (Weber–Morris) diffusion model [54]. Based on the present study, the transport or the movement of 4-chlorophenol molecules from the bulk solution to hydrogel beads' mesoporous surface could be deemed the slowest step, hence the rate-determining step. Thus, the intra-particle diffusion model

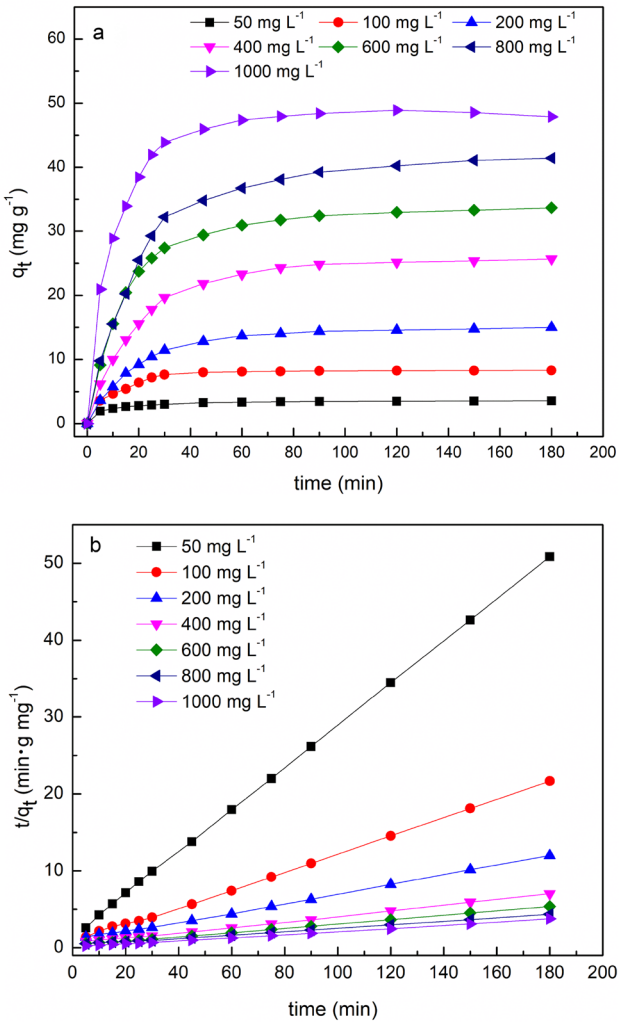

Fig. 7 **a** Plot of q_t vs. time for various 4-CP concentrations and **b** pseudo-second-order (model I) kinetic model fitting for batch adsorption of 4-chlorophenol of various initial 4-CP concentrations on CTAC-CNC/ALG hydrogel beads (Conditions: sorbent dosage = 1.0 g; stirring speed = 400 rpm; T = 30 °C; pH 2)

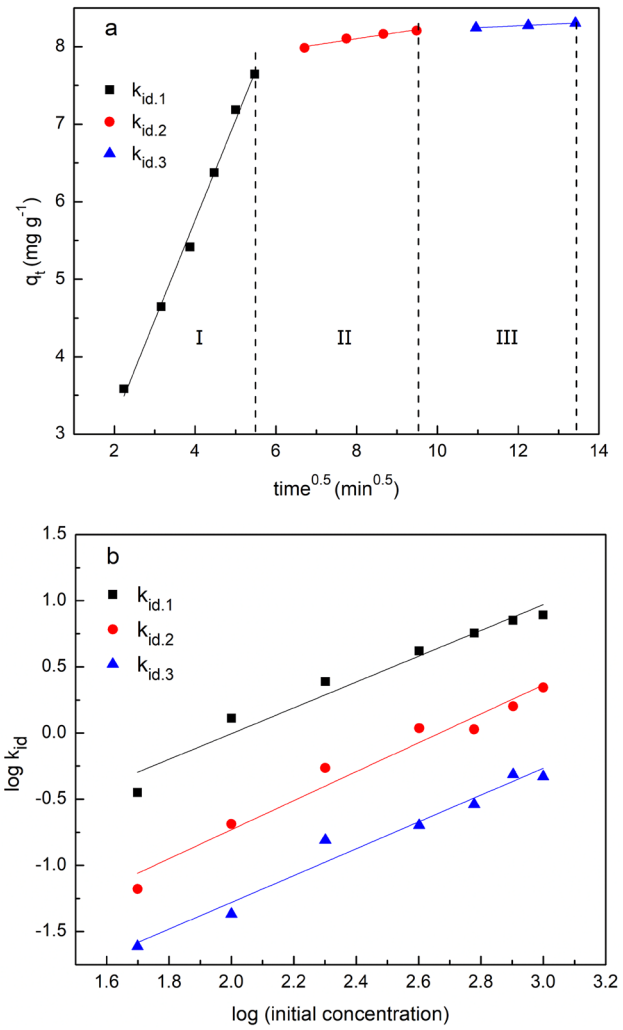

Fig. 8 **a** Weber–Morris plots for batch adsorption of 100 mg L^{-1}. 4-CP solution onto CTAC-CNC/ALG hydrogel beads and **b** plot of log kid against log (initial 4-CP concentration) (Conditions: sorbent dosage = 1.0 g; stirring speed = 400 rpm; T = 30 °C; pH 2)

was employed to fit the experimental data further to interpret the adsorption of 4-CP onto prepared hydrogel beads. According to the q_t versus $t^{0.5}$ regression plot (Fig. 8a), three distinct regions with different slopes (multi-step nature) can be identified, which elucidate the mass transfer of 4-CP into CTAC-CNC/ALG@HB. These three intraparticle diffusion constants have been denoted as $k_{id.1}$, $k_{id.2}$ and $k_{id.3,}$ which define the diffusion rates at different phases of the adsorption process established from the three slopes, each conforming to one diffusion behaviour.

Table S4 depicts the numerical values of each intraparticle diffusion constant. The rate constants were in the order of; $k_{id.1} > k_{id.2} > k_{id.3}$, implying the contribution of a rapid initial stage of external mass transfer, a slower second phase (boundary layer diffusion), and a much sluggish third stage of diffusion as shown in Fig. 8a. More than 50% of 4-CP molecules get transported from the bulk solution to the hydrogel bead surface during the initial stage. Once the external hydrogel bead surface gets saturated, 4-CP molecules begin to occupy microstructures and pores, represented by the second stage. A lower diffusion rate ($k_{id,2}$) in the second stage corresponds to an increased diffusion resistance exposed by the pores. The third phase exemplifies a much slower diffusion rate ($k_{id,3}$) of 4-CP molecules into the internal surface of hydrogel beads, and ultimately the diffusion reaches an equilibrium. According to intraparticle diffusion plots, the value of C is not 0, signifying the occurrence of some degree of boundary layer control. Since the regression plots of q_t versus $t^{0.5}$ for all three regions were not linear and did not intersect the origin, intraparticle/pore diffusion was not the sole rate-limiting step in the adsorption process.

Based on Table S4, it is evident that increased initial 4-CP concentration resulted in an increased rate of diffusion. Hence, Fig. 8b has been plotted by correlating the logarithmic values of each $k_{id.1}$, $k_{id.2}$ and $k_{id.3}$ rate parameters with the logarithmic values of initial 4-CP concentration. Thus, intraparticle-diffusion study revealed that 4-CP molecules migrated from solution's bulk phase to the external surface of CTAC-CNC/ALG hydrogel beads. Subsequently, 4-CP molecules diffused within the interlayer pores (intraparticle diffusion) of CTAC-CNC/ALG hydrogel beads and finally the occurrence of rapid chemical bonding (mainly electrostatic attraction and H-bonding) between 4-CP molecules and the interior surfaces of CTAC-CNC/ALG hydrogel beads.

SEM–EDX Analysis

Possible interactions of 4-CP uptake by CTAC-CNC/ALG@HB were assessed through SEM-energy dispersive X-ray spectroscopy (EDX) by analyzing the differences in the element content of the hydrogel bead surface before and after 4-CP adsorption (Figure S4). Before adsorption, CTAC-CNC/ALG@HB reported atomic percentages of C, O, N, Ca, Cl and Na elements, which are 50.30, 39.07, 5.68, 3.51, 0.91 and 0.39%, respectively. The insignificant amount of Na content (0.39%) present in the EDX spectrum before adsorption suggests effective crosslinking of Na^+ ions in the sodium alginate matrix with Ca^{2+} crosslinker ions. The presence of 0.91% of Cl content corroborates the coordinated bonding between N^+ and Cl^- in CTAC cationic surfactant and Cl^- ions from $CaCl_2$ crosslinking agent, while the presence of 5.68% of N element affirms the successful surface modification of CNCs with CTAC. After 4-CP uptake, the atomic % of Cl element raised to 3.35%, justifying the adsorption of 4-chlorophenol onto CTAC-CNC/ALG@HB. It can also be noticed that the O atomic content showed a slight increment upon 4-CP adsorption and a minor reduction in N content, which could be a result of 4-CP molecules occupying the surface active sites of hydrogel beads. Since SEM images affirmed the porous structure of the fabricated hydrogel beads (also shown in Fig. 3), one of the feasible mechanisms of 4-CP adsorption could be through adsorptive pore-filling. Yasir et al. [55] attested that one probable route for phenol adsorption on ionic liquid-agar-alginate beads could advance through the adsorptive pore-filling mechanism.

XPS Analysis

A comparison of the wide-scan spectra (survey spectra) of the hydrogel beads acquired before and after adsorption disclosed the efficient loading of 4-chlorophenol onto hydrogel microspheres, which is apparent from the appearance of a prominent Cl 2p peak positioned at 198.40 eV as shown in Fig. 9a. The noticeable increment in O and Cl atomic content after 4-CP adsorption also reinforces the data obtained from SEM–EDX analysis, upholding successful 4-CP uptake. Figure 9b depicts the doublet peaks of Ca $2p_{3/2}$ and Ca $2p_{1/2}$ with a splitting of 3.49 eV, in which the Ca $2p_{3/2}$ signal (347.39 eV) represents the crosslinking of Ca^{2+} ions with $–COO^-$ groups. It was evident that the intensities of Ca peaks representative of Ca^+ reduced to a certain extent, and a clear shift in peak positions to higher binding energies following 4-CP adsorption, which may be due to a possible interaction of crosslinked Ca^{2+} with 4-CP. Pertaining to the C 1s spectrum of CTAC-CNC/ALG@HB shown in Fig. 9c, the binding energies of COO^-, C=O, and C–O groups are 287.57, 286.20 and 284.62 eV [12, 39], respectively. C=O and C–O peaks correspond to –COOH and –OH groups of alginate and CNC in the hydrogel beads, agreeing with the results obtained from FTIR spectroscopy. It can be noticed that following 4-CP adsorption, there was a slight shift in the binding energies of C=O and C–O peaks to 286.21 and 287.59 eV, respectively, revealing the involvement of –COOH and –OH groups in the adsorption process [47].

O 1s spectra of CTAC-CNC/ALG@HB (Fig. 8d) affirmed that COO^- (532.82 eV), C=O (531.18 eV), and C–O (532.31 eV) signals shifted slightly lower binding energies 532.57, 531.15 and 532.29 eV, respectively. In addition, the signal intensity of the C-O bond was reduced upon 4-CP uptake, suggesting the contribution of carboxyl groups during crosslinking and binding of 4-CP. Hu et al. [12] reported a similar observation. The presence of the quaternary ammonium group pertaining to CTAC modification was further validated through XPS analysis, as shown in Fig. 9a survey spectrum. The high-resolution N spectrum of CTAC-CNC/ALG@HB (Fig. 9e) demonstrated two distinct peaks at 399.77 eV and 402.30 eV, referring to N atom bonded to a C atom via a single bond and nitrogen of $(CH_3)_3N^+$ group in CTAC [27], respectively, affirming the chemical connection between 4-CP and $(CH_3)_3N^+$. Thus, XPS analysis revealed the involvement of $(CH_3)_3N^+$, carboxyl, and hydroxyl groups, acting as surface active sites in CTAC-CNC/ALG hydrogel beads in the adsorption process.

Another route for the binding mechanism could be via the intermolecular forces between 4-chlorophenol and CTAC-CNC/ALG@HB, which has also been proven through thermodynamic, equilibrium isotherm and kinetic studies. Apart from Vander Waals forces, these intermolecular forces could be hydrogen-bonding, electrostatic attraction and π–π stacking as depicted in Fig. 10.

Based on XPS analysis, a mechanism of adsorption has been proposed (Fig. 10), which is primarily governed by H-bonding and electrostatic attraction between 4-CP molecules and the trimethyl groups ($(CH_3)_3N^+$) of the quaternary ammonium salt, carboxyl (–COOH) and hydroxyl (OH)

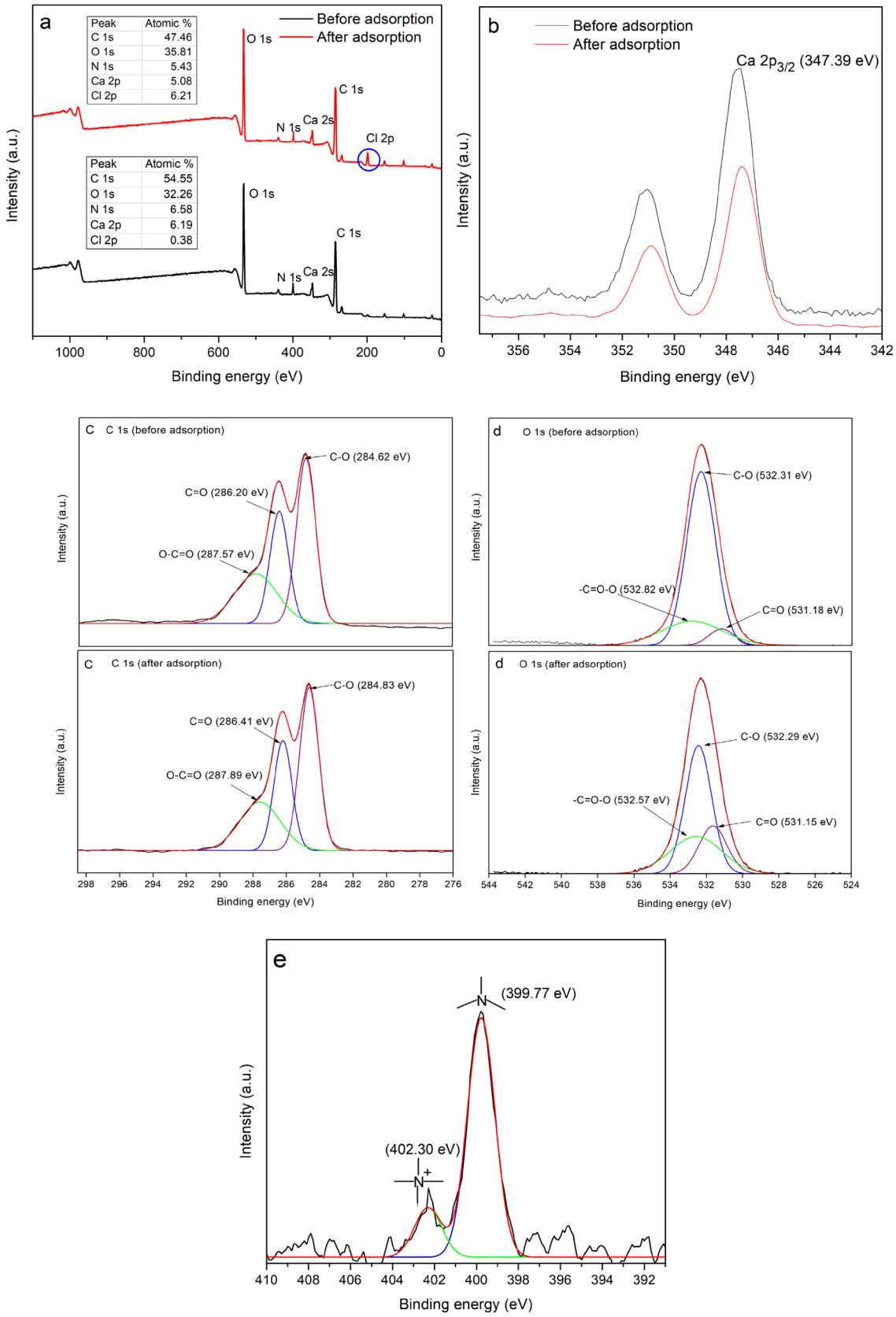

Fig. 9 The XPS analysis of CTAC-CNC/ALG hydrogel beads before and after 4-chlorophenol adsorption: **a** wide-scan spectra and high-resolution spectra of; **b** Ca 2p, **c** C 1 s, **d** O 1 s and **e** N 1 s

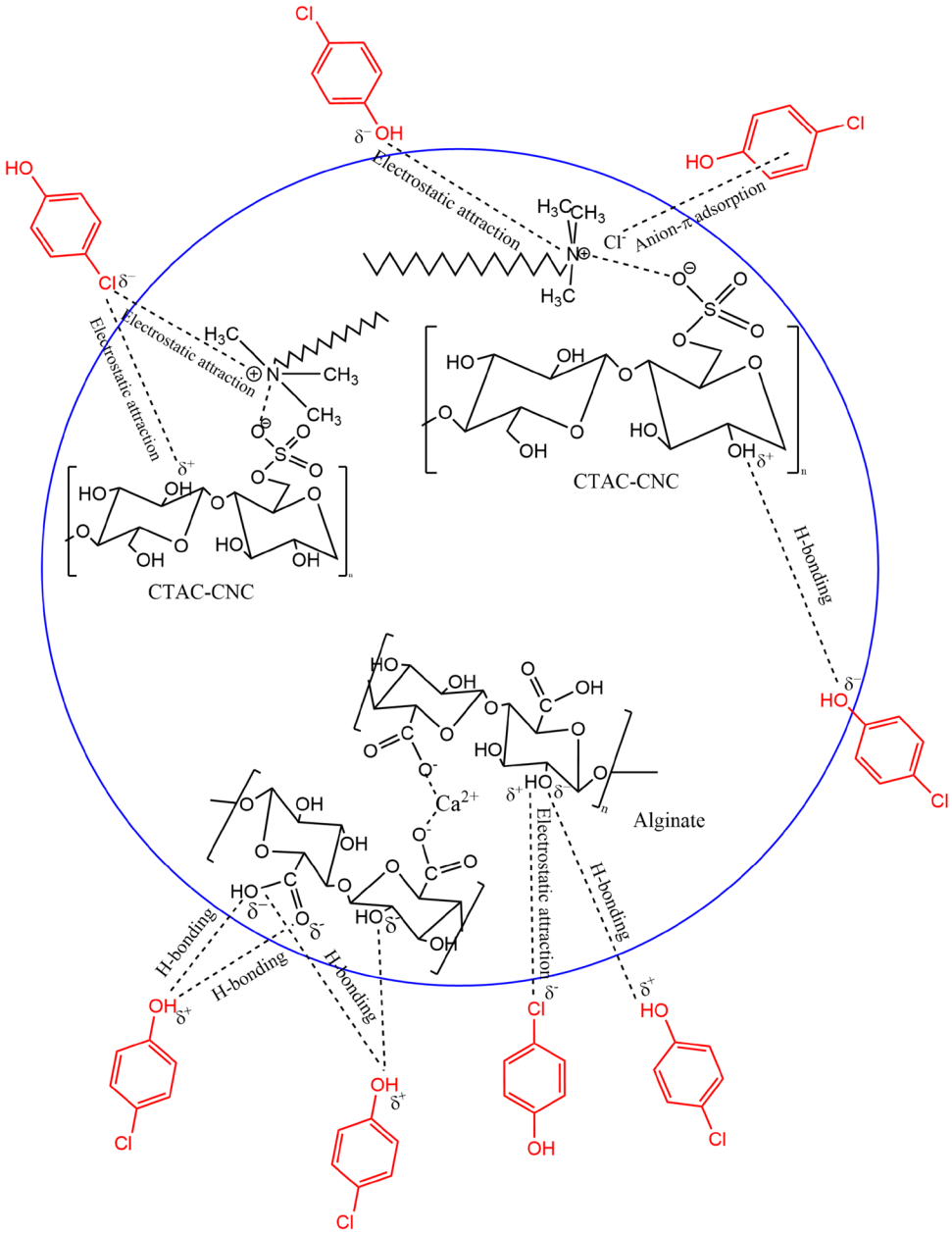

Fig. 10 Proposed mechanism of adsorption depicting the interaction forces between CTAC-CNC/ALG hydrogel beads with 4-chlorophenol

groups of the fabricated CNC-based hydrogel beads. Since alginate and CNC have many binding (active) sites, establishing H-bonding between these sites and hydrophilic 4-CP molecules is inevitable. Oxygen atoms of ketone groups present in alginate and oxygen atoms of SO_3^- groups present in CNC could also interact with -OH groups of 4-CP. Besides, ion-induced dipole interaction could occur between Cl^- ions of CTAC and the pi-electrons of the 4-chlorophenol ring (anion-π stacking). In relation to pH_{pzc}, at medium pH lower than of pH_{pzc}, the hydroxyl (in ALG and CNC) and carboxyl (ALG) groups on CTAC-CNC/ALG@HB are protonated due to high H^+ concentration in the medium which can electrostatically interact with 4-CP. The large number of hydroxyl groups in the hydrogel beads would be protonated at pH < 6.76, rendering the surface positive charged. Since the pK_a of –COO– on alginate ranges from 3 to 5 [3], overall negative surface charge of alginate is reduced as the solution pH approaches pK_a of -COO-, making COOH groups bind with 4-CP through H-bonding and electrostatic attraction.

Reusability Performance

Since the raw materials employed to produce viable adsorbents are agricultural wastes, for instance, oil palm biomass, they are rather improbable to instigate secondary pollution. Nevertheless, regenerating adsorbents prepared

by exploiting agricultural wastes is a challenge [66]. Recyclability is one of the critical criteria for the productive commercialization of new adsorbents in wastewater treatment. Hence, the regeneration of adsorbents plays a pivotal role in expanding their economic value. In their comprehensive review, Dutta and co-authors [67] noted that the thermal regeneration method perturbs the vital surface characteristics of adsorbents through polymerization, decomposition, and oxidation as a result of applying high temperatures during the heat treatment process. Therefore, the present study adopted a solvent-assisted (chemical) regeneration approach for recycling exhausted hydrogel beads. To regenerate the spent adsorbent, the hydrogel beads were added to ethanol and agitated for 24 h at 30 °C and then reused. Wang et al. [68] noted that ethanol being a dipolar solvent, can diminish hydrophobic interactions between adsorbate molecules and the adsorbent. The results pointed out that porous CTAC-CNC/alginate hydrogel beads could retain up to 78.65% of their initial (maximum) adsorption capacity even after five adsorption–desorption cycles (Fig. 11). This indicates that the CTAC-CNC/ALG@HB could be an efficient, cost-effective, and reusable adsorbent for the removal of 4-chlorophenol from wastewater. Since the adsorption of 4-CP on CTAC-CNC/ALG@HB surface primarily proceeded via physical adsorption, 4-CP molecules could be readily desorbed than those that are chemisorbed, hence a higher efficiency of recyclability was achieved.

Performance Evaluation

The comparison of Langmuir's maximum adsorption capacity (q_{max}) and experimental conditions of numerous adsorbents for 4-chlorophenol removal is presented in Table 4.

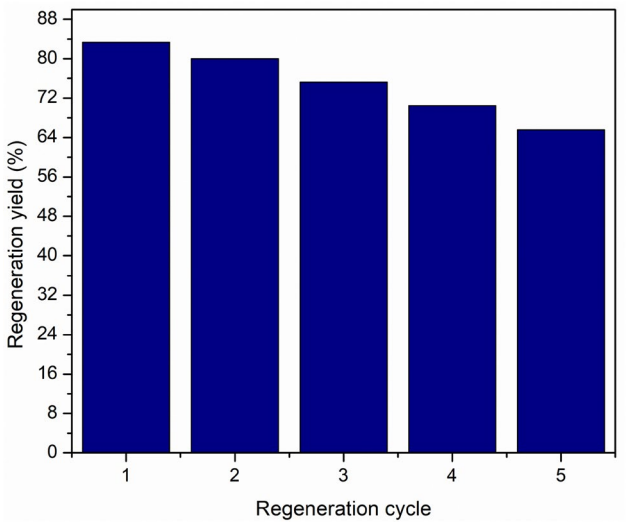

Fig. 11 Regeneration yield of porous CTAC-CNC/ALG hydrogel beads corresponding to 4-CP adsorption from wastewater

The Langmuir q_m value of porous CTAC-CNC/ALG@HB was 64.94 mg g^{-1}. The findings revealed that porous CTAC-CNC/ALG@HB employed in the present study offer comparable or better 4-chlorophenol adsorptive removal capacity over most of the other sorbents employed in past studies. The higher adsorption capability of fabricated hydrogel beads could owe to two significant factors: the generation of surface active sites for 4-CP adsorption onto the polymer matrix by incorporating CTAC-modified CNCs and increasing the porous structure, which expands the surface area of the polymer matrix. Thus, enhanced surface area results in the availability of more surface active sites, thereby improving its adsorption capacity. The comparative profile proposes that porous CTAC-CNC/ALG@HB could be a potential adsorbent for 4-chlorophenol removal in wastewater, owing to their biocompatible nature, low-cost, ease of preparation and cost-effective regeneration.

Conclusion

Porous CTAC-CNC/ALG@HB were prepared through a polyelectrolyte complexation and employed to adsorb 4-chlorophenol from wastewater. The fabrication process involved facile ionotropic gelation using $CaCl_2$ as the crosslinker agent to yield robust CTAC-CNC/ALG@HB at a lower cost. CNC-based hydrogel beads exhibited a high adsorption efficiency towards 4-chlorophenol by dint of the cationic modification of CNC using surfactant impregnation and its relatively high porosity. The influence of various factors was studied during the adsorption experiments. Notably, the adsorptive removal capacity of 4-chlorophenol was enhanced with CTAC-CNC/ALG@HB dosage, contact time, and initial 4-CP concentration, among other factors, where 64.94 mg g^{-1} was attained as the maximum uptake for 4-CP. The thermodynamic and kinetic data affirmed that the adsorption mechanism is exothermic and the adsorption kinetics accorded with the pseudo-second-order kinetics. Intra-particle diffusion model revealed that the rate-determining step was not only controlled by pore diffusion. The adsorption mechanisms leading to an effective adsorption process were adsorptive pore-filling, hydrogen-bonding, electrostatic interaction, anion-π and π–π stacking. In addition, 4-chlorophenol uptake best fitted the Langmuir adsorption isotherm model, and the hydrogel beads offered adequate adsorption capacity even after five regeneration cycles.

Table 4 Comparison of adsorbents utilized for 4-chlorophenol adsorption from wastewater

Adsorbent	Initial 4-CP concentration ($mg\ L^{-1}$)	Adsorbent dose ($g\ L^{-1}$)	Temperature (°C)	Medium pH	Contact time (h)	Isotherm model	q_{max} ($mg\ g^{-1}$)	Kinetic model	References
Dried anaerobic digested sludge	30	5	25 ± 1	3	4	Freundlich	1.01	PFO	[69]
Hard coal	38.5	20	25	2.5	2	Langmuir	2.86	PSO	[70]
Rice bran ash	400	2.5	–	5	4	Freundlich	4.30	PSO	[71]
Cystoseirain-dica brown algae biomass	400	2.5	–	7	2	Freundlich	2.34	PSO	
Ethylen-ediamine rosin-based resin	20	0.8	20	6	24	Langmuir	9.38	–	[72]
HDTMA surfactant modified zeolite	50	20	20	–	24	Freundlich	12.70	PSO	[65]
BDTDA surfactant modified zeolite	50	20	20	–	24	Freundlich	6.41	PSO	
HNO_3 treated-coconut shell charcoal	25	13.5	25	2	1	Langmuir	23.13	PSO	[73]
Amberlite XAD-4 macro-reticular polymeric resin	100	10	25	6.8–6.9	2	Redlich-Peterson	27.91	PSO	[74]
Multi-walled carbon nanotubes	64.2	1.5	25	–	2	Freundlich	32.9	PSO	[75]
Bamboo charcoal derived-nanosized activated carbon	100	–	25	7	10	Freundlich	79.69	PSO	[76]
Magnetic porous resorcinol-melamine–formal-dehyde based resin grafted chitosan beads	150	24	25	9	11.67	Langmuir	99	PSO	[53]

Table 4 (continued)

Adsorbent	Initial 4-CP concentration (mg L^{-1})	Adsorbent dose (g L^{-1})	Temperature (°C)	Medium pH	Contact time (h)	Isotherm model	q_{max} (mg g^{-1})	Kinetic model	References
Porous CTAC-CNC/alginate hydrogel beads	100	10	30	4	6	Langmuir	64.94	PSO	Present study

PFO Pseudo-first-order, *PSO* Pseudo-second-order

Supplementary Information The online version contains supplementary material available at https://doi.org/10.1007/s10924-022-02573-4.

Acknowledgements The authors are grateful to Universiti Sains Malaysia for the financial assistance obtained through the Research University Incentive, RUI Grant (1001/PKIMIA/8011077) and USM External Grant (304/PKIMIA/6501094/I129).

Author Contributions TSH: Methodology, Software, Data collection and analysis, Investigation, Writing-original draft, Writing-review & editing. RA: Project administration, Validation, Writing-review & editing. MKMH: Formal analysis, Data curation, Visualization. MHH: Conceptualization, Resources, Supervision, Project administration, Funding acquisition, Writing-review & editing.

Funding Research University Incentive, RUI Grant (1001/PKIMIA/8011077) and USM External Grant (304/PKIMIA/6501094/I129).

Data Availability The raw/processed data required to reproduce these findings cannot be shared at this time as the data also forms part of an ongoing study.

Declarations

Conflict of interest The authors declare that they have no known competing financial interests or personal relationships that could have appeared to influence the work reported in this paper.

Ethics Approval and Consent to Participate This article does not contain any studies with animals performed by any of the authors. All authors have agreed with the content and that all gave explicit consent to submit and participate.

Consent for Publication On behalf of authors, Assoc. Prof. Dr. M. Hazwan Hussin has been given authorization to submit and correspond. All authors read and approved the final manuscript.

References

1. Mohsenpour SF, Hennige S, Willoughby N, Adeloye A, Gutierrez T (2021) Integrating micro-algae into wastewater treatment: a review. Sci Total Environ. https://doi.org/10.1016/j.scitotenv.2020.142168
2. Cheng M, Zeng G, Huang D, Lai C, Liu Y, Zhang C, Wang R, Qin L, Xue W, Song B (2018) High adsorption of methylene blue by salicylic acid-methanol modified steel converter slag and evaluation of its mechanism. J Colloid Interface Sci 515:232–239. https://doi.org/10.1016/j.jcis.2018.01.008
3. Mohammed N, Grishkewich N, Berry RM, Tam KC (2015) Cellulose nanocrystal-alginate hydrogel beads as novel adsorbents for organic dyes in aqueous solutions. Cellulose 22(6):3725–3738. https://doi.org/10.1007/s10570-015-0747-3
4. Wang X, Peng R, He H, Yan X, Zhu S, Zhao H, Deng D, Qiongwei Y, Lei Y, Luo L (2018) Nanomagnetic polyhedral oligomeric silsesquioxanes composite derived sulfur-containing adsorbents for effective elimination of hexavalent chromium and organic cationic dyes from water. Colloid Surf A 550:1–8. https://doi.org/10.1016/j.colsurfa.2018.04.019
5. Zhang Z, Sun D, Li G, Zhang B, Zhang B, Qiu S, Li Y, Wu T (2019) Calcined products of Mg-Al layered double hydroxides/single-walled carbon nanotubes nanocomposites for expeditious removal of phenol and 4-chlorophenol from aqueous solutions. Colloid Surf A 565:143–153. https://doi.org/10.1016/j.colsurfa.2019.01.001
6. Lei M, Gao Q, Zhou K, Gogoi P, Liu J, Wang J, Song H, Wang S, Liu X (2021) Catalytic degradation and mineralization mechanism of 4-chlorophenol oxidized by phosphomolybdic acid/H_2O_2. Sep Purif Technol. https://doi.org/10.1016/j.seppur.2020.117933
7. Wen Q, Yang T, Wang S, Chen Y, Cong L, Qu Y (2013) Dechlorination of 4-chlorophenol to phenol in bioelectrochemical systems. J Hazard Mater 244–245:743–749. https://doi.org/10.1016/j.jhazmat.2012.11.002
8. Chuein ALH, Idris NN, Hamidon TS, Mohd Azani NFS, Abdullah NS, Sharifuddin SS, Ying AS, Hussin MH (2021) Kinetics and equilibrium studies of methylene blue dye adsorption on oil palm frond adsorbent. Desalin Water Treat 216:358–371. https://doi.org/10.5004/dwt.2021.26795
9. Singh NB, Nagpal G, Agrawal S, Rachna (2018) Water purification by using adsorbents: a review. Environ Technol Innov 11:187–240. https://doi.org/10.1016/j.eti.2018.05.006
10. Crini G, Lichtfouse E, Wilson LD, Morin-Crini N (2019) Conventional and non-conventional adsorbents for wastewater treatment. Environ Chem Lett 17(1):195–213. https://doi.org/10.1007/s10311-018-0786-8
11. Hamidon TS, Adnan R, Haafiz MKM, Hussin MH (2022) Cellulose-based beads for the adsorptive removal of wastewater effluents: a review. Environ Chem Lett 20:1965–2017. https://doi.org/10.1007/s10311-022-01401-4
12. Hu Z-H, Omer AM, Ouyang Xk YuD (2018) Fabrication of carboxylated cellulose nanocrystal/sodium alginate hydrogel beads for adsorption of Pb(II) from aqueous solution. Int J Biol Macromol 108:149–157. https://doi.org/10.1016/j.ijbiomac.2017.11.171

13. Mahfoudhi N, Boufi S (2017) Nanocellulose as a novel nanostructured adsorbent for environmental remediation: a review. Cellulose 24(3):1171–1197. https://doi.org/10.1007/s10570-017-1194-0
14. Trache D, Tarchoun AF, Derradji M, Hamidon TS, Masruchin N, Brosse N, Hussin MH (2020) Nanocellulose: from fundamentals to advanced applications. Front Chem. https://doi.org/10.3389/fchem.2020.00392
15. Diyanilla R, Hamidon TS, Suryanegara L, Hussin MH (2020) Overview of pretreatment methods employed on oil palm biomass in producing value-added products: a review. BioResources 15(4):9935–9997. https://doi.org/10.15376/biores.15.4.Diyanilla
16. Thomas B, Raj MC, Joy J, Moores A, Drisko GL, Sanchez C (2018) Nanocellulose, a versatile green platform: from biosources to materials and their applications. Chem Rev 118(24):11575–11625. https://doi.org/10.1021/acs.chemrev.7b00627
17. Hastati DY, Hambali E, Syamsu K, Warsiki E (2021) Enhanced hydrophobicity of nanofibrillated cellulose through surface modification using cetyltrimethylammonium chloride derived from palmityl alcohol. Waste Biomass Valor 12(9):5147–5159. https://doi.org/10.1007/s12649-021-01366-5
18. Tardy BL, Yokota S, Ago M, Xiang W, Kondo T, Bordes R, Rojas OJ (2017) Nanocellulose-surfactant interactions. Curr Opin Colloid Interface Sci 29:57–67. https://doi.org/10.1016/j.cocis.2017.02.004
19. Feizi ZH, Fatehi P (2021) Interaction of hairy carboxyalkyl cellulose nanocrystals with cationic surfactant: effect of carbon spacer. Carbohydr Polym. https://doi.org/10.1016/j.carbpol.2020.117396
20. Seweryn A (2018) Interactions between surfactants and the skin -theory and practice. Adv Colloid Interface Sci 256:242–255. https://doi.org/10.1016/j.cis.2018.04.002
21. Melikoğlu AY, Bilek SE, Cesur S (2019) Optimum alkaline treatment parameters for the extraction of cellulose and production of cellulose nanocrystals from apple pomace. Carbohydr Polym 215:330–337. https://doi.org/10.1016/j.carbpol.2019.03.103
22. Rahmani Z, Sahraei R, Ghaemy M (2018) Preparation of spherical porous hydrogel beads based on ion-crosslinked gum tragacanth and graphene oxide: study of drug delivery behavior. Carbohydr Polym 194:34–42. https://doi.org/10.1016/j.carbpol.2018.04.022
23. Supramaniam J, Adnan R, Mohd Kaus NH, Bushra R (2018) Magnetic nanocellulose alginate hydrogel beads as potential drug delivery system. Int J Biol Macromol 118:640–648. https://doi.org/10.1016/j.ijbiomac.2018.06.043
24. Fan L, Lu Y, Yang L-Y, Huang F, Ouyang X-k (2019) Fabrication of polyethylenimine-functionalized sodium alginate/cellulose nanocrystal/polyvinyl alcohol core-shell microspheres ((PVA/SA/CNC)@PEI) for diclofenac sodium adsorption. J Colloid Interface Sci 554:48–58. https://doi.org/10.1016/j.jcis.2019.06.099
25. Dungani R, Owolabi AF, Saurabh CK, Abdul Khalil HPS, Tahir PM, Hazwan CICM, Ajijolakewu KA, Masri MM, Rosamah E, Aditiawati P (2017) Preparation and fundamental characterization of cellulose nanocrystal from oil palm fronds biomass. J Polym Environ 25(3):692–700. https://doi.org/10.1007/s10924-016-0854-8
26. Salajková M, Berglund LA, Zhou Q (2012) Hydrophobic cellulose nanocrystals modified with quaternary ammonium salts. J Mater Chem 22(37):19798–19805. https://doi.org/10.1039/C2JM34355J
27. Ma Q, Cao L, Liang T, Li J, Lucia LA, Wang L (2018) Active tara gum/PVA blend films with curcumin-loaded CTAC brush-TEMPO-oxidized cellulose nanocrystals. ACS Sustain Chem Eng 6(7):8926–8934. https://doi.org/10.1021/acssuschemeng.8b01281
28. Abitbol T, Kloser E, Gray DG (2013) Estimation of the surface sulfur content of cellulose nanocrystals prepared by sulfuric acid hydrolysis. Cellulose 20(2):785–794. https://doi.org/10.1007/s10570-013-9871-0
29. Hua S, Ma H, Li X, Yang H, Wang A (2010) pH-sensitive sodium alginate/poly(vinyl alcohol) hydrogel beads prepared by combined Ca^{2+} crosslinking and freeze-thawing cycles for controlled release of diclofenac sodium. Int J Biol Macromol 46(5):517–523. https://doi.org/10.1016/j.ijbiomac.2010.03.004
30. Ren H, Gao Z, Wu D, Jiang J, Sun Y, Luo C (2016) Efficient Pb (II) removal using sodium alginate-carboxymethyl cellulose gel beads: Preparation, characterization, and adsorption mechanism. Carbohydr Polym 137:402–409. https://doi.org/10.1016/j.carbpol.2015.11.002
31. Xu Y, Zhan C, Fan L, Wang L, Zheng H (2007) Preparation of dual crosslinked alginate-chitosan blend gel beads and in vitro controlled release in oral site-specific drug delivery system. Int J Pharm 336(2):329–337. https://doi.org/10.1016/j.ijpharm.2006.12.019
32. Kumar NS, Min K (2011) Phenolic compounds biosorption onto Schizophyllum commune fungus: FTIR analysis, kinetics and adsorption isotherms modeling. Chem Eng J 168(2):562–571. https://doi.org/10.1016/j.cej.2011.01.023
33. Suresh S, Srivastava VC, Mishra IM (2013) Studies of adsorption kinetics and regeneration of aniline, phenol, 4-chlorophenol and 4-nitrophenol by activated carbon. Chem Ind Chem Eng Q 19(2):195–212. https://doi.org/10.2298/CICEQ111225054S
34. Shan S, Tang H, Zhao Y, Wang W, Cui F (2019) Highly porous zirconium-crosslinked graphene oxide/alginate aerogel beads for enhanced phosphate removal. Chem Eng J 359:779–789. https://doi.org/10.1016/j.cej.2018.10.033
35. Qiusheng Z, Xiaoyan L, Jin Q, Jing W, Xuegang L (2015) Porous zirconium alginate beads adsorbent for fluoride adsorption from aqueous solutions. RSC Adv 5(3):2100–2112. https://doi.org/10.1039/C4RA12036A
36. Karzar Jeddi M, Mahkam M (2019) Magnetic nano carboxymethyl cellulose-alginate/chitosan hydrogel beads as biodegradable devices for controlled drug delivery. Int J Biol Macromol 135:829–838. https://doi.org/10.1016/j.ijbiomac.2019.05.210
37. Hu Y, Tang L, Lu Q, Wang S, Chen X, Huang B (2014) Preparation of cellulose nanocrystals and carboxylated cellulose nanocrystals from borer powder of bamboo. Cellulose 21(3):1611–1618. https://doi.org/10.1007/s10570-014-0236-0
38. Diao H, Zhang Z, Liu Y, Song Z, Zhou L, Duan Y, Zhang J (2020) Facile fabrication of carboxylated cellulose nanocrystal-MnO_2 beads for high-efficiency removal of methylene blue. Cellulose 27(12):7053–7066. https://doi.org/10.1007/s10570-020-03260-0
39. Xu X, Ouyang X-k, Yang L-Y (2021) Adsorption of Pb(II) from aqueous solutions using crosslinked carboxylated chitosan/carboxylated nanocellulose hydrogel beads. J Mol Liq. https://doi.org/10.1016/j.molliq.2020.114523
40. Albayati TM, Jassam AAA (2019) Synthesis and characterization of mesoporous materials as a carrier and release of prednisolone in drug delivery system. J Drug Deliv Sci Technol. https://doi.org/10.1016/j.jddst.2019.101176
41. Luo X, Lei X, Cai N, Xie X, Xue Y, Yu F (2016) Removal of heavy metal ions from water by magnetic cellulose-based beads with embedded chemically modified magnetite nanoparticles and activated carbon. ACS Sustain Chem Eng 4(7):3960–3969. https://doi.org/10.1021/acssuschemeng.6b00790
42. Ding Y, Song C, Gong W, Liu L, Wu M, Li L, Yao J (2021) Robust, sustainable, hierarchical multi-porous cellulose beads via pre-crosslinking strategy for efficient dye adsorption. Cellulose 10:1–15. https://doi.org/10.1007/s10570-021-03979-4
43. Idris NN, Hamidon TS, Abdullah NS, Suryanegara L, Hussin MH (2022) Potential of oil palm frond cellulose nanocrystals-activated carbon hydrogel beads for the removal of paracetamol from aqueous media. Cellulose 29:1583–1607. https://doi.org/10.1007/s10570-021-04379-4

44. Harada N, Mitsukami Y, Uyama H (2021) Preparation and characterization of water-swellable hydrogel-forming porous cellulose beads. Polymer. https://doi.org/10.1016/j.polymer.2021.123381
45. Li B, Pan Y, Zhang Q, Huang Z, Liu J, Xiao H (2019) Porous cellulose beads reconstituted from ionic liquid for adsorption of heavy metal ions from aqueous solutions. Cellulose 26(17):9163–9178. https://doi.org/10.1007/s10570-019-02687-4
46. Yang H-R, Li S-S, Shan X-C, Yang C, An Q-D, Zhai S-R, Xiao Z-Y (2022) Hollow polyethyleneimine/carboxymethyl cellulose beads with abundant and accessible sorption sites for ultra-efficient chromium (VI) and phosphate removal. Sep Purif Technol. https://doi.org/10.1016/j.seppur.2021.119607
47. Zhao H, Ouyang X-K, Yang L-Y (2021) Adsorption of lead ions from aqueous solutions by porous cellulose nanofiber-sodium alginate hydrogel beads. J Mol Liq. https://doi.org/10.1016/j.molliq.2020.115122
48. Jamali M, Akbari A (2021) Facile fabrication of magnetic chitosan hydrogel beads and modified by interfacial polymerization method and study of adsorption of cationic/anionic dyes from aqueous solution. J Environ Chem Eng. https://doi.org/10.1016/j.jece.2021.105175
49. Xia F, Yang H, Li L, Ren Y, Shi D, Chai H, Ai H, He Q, Gu L (2020) Enhanced nitrate adsorption by using cetyltrimethylammonium chloride pre-loaded activated carbon. Environ Technol 41(27):3562–3572. https://doi.org/10.1080/09593330.2019.1615133
50. Hu B, Luo H (2010) Adsorption of hexavalent chromium onto montmorillonite modified with hydroxyaluminum and cetyltrimethylammonium bromide. Appl Surf Sci 257(3):769–775. https://doi.org/10.1016/j.apsusc.2010.07.062
51. Shen Y-H (2004) Phenol sorption by organoclays having different charge characteristics. Colloids Surf A Physicochem Eng Asp 232(2):143–149. https://doi.org/10.1016/j.colsurfa.2003.10.014
52. Mangrulkar PA, Kamble SP, Meshram J, Rayalu SS (2008) Adsorption of phenol and o-chlorophenol by mesoporous MCM-41. J Hazard Mater 160(2):414–421. https://doi.org/10.1016/j.jhazmat.2008.03.013
53. Heydaripour J, Gazi M, Oladipo AA, Gulcan HO (2019) Porous magnetic resin-g-chitosan beads for adsorptive removal of phenolic compounds. Int J Biol Macromol 123:1125–1131. https://doi.org/10.1016/j.ijbiomac.2018.11.168
54. Hameed BH, Chin LH, Rengaraj S (2008) Adsorption of 4-chlorophenol onto activated carbon prepared from rattan sawdust. Desalination 225(1):185–198. https://doi.org/10.1016/j.desal.2007.04.095
55. Yasir N, Khan AS, Hassan MF, Ibrahim TH, Khamis MI, Nancarrow P (2022) Ionic liquid agar-alginate beads as a sustainable phenol adsorbent. Polymers 14(5):984. https://doi.org/10.3390/polym14050984
56. Nadavala SK, Swayampakula K, Boddu VM, Abburi K (2009) Biosorption of phenol and o-chlorophenol from aqueous solutions on to chitosan-calcium alginate blended beads. J Hazard Mater 162(1):482–489. https://doi.org/10.1016/j.jhazmat.2008.05.070
57. Madannejad S, Rashidi A, Sadeghhassani S, Shemirani F, Ghasemy E (2018) Removal of 4-chlorophenol from water using different carbon nanostructures: a comparison study. J Mol Liq 249:877–885. https://doi.org/10.1016/j.molliq.2017.11.089
58. Bhomick PC, Supong A, Baruah M, Pongener C, Gogoi C, Sinha D (2020) Alizarin Red S adsorption onto biomass-based activated carbon: optimization of adsorption process parameters using Taguchi experimental design. Int J Environ Sci Technol 17(2):1137–1148. https://doi.org/10.1007/s13762-019-02389-1
59. Sujana MG, Mishra A, Acharya BC (2013) Hydrous ferric oxide doped alginate beads for fluoride removal: adsorption kinetics and equilibrium studies. Appl Surf Sci 270:767–776. https://doi.org/10.1016/j.apsusc.2013.01.157
60. Srivastav AL, Singh PK, Srivastava V, Sharma YC (2013) Application of a new adsorbent for fluoride removal from aqueous solutions. J Hazard Mater 263:342–352. https://doi.org/10.1016/j.jhazmat.2013.04.017
61. Oladipo AA, Ifebajo AO, Vaziri R (2018) Green adsorbents for removal of antibiotics, pesticides and endocrine disruptors. In: Crini G, Lichtfouse E (eds) Green adsorbents for pollutant removal: innovative materials. Springer, Cham
62. Salleh MAM, Mahmoud DK, Karim WAWA, Idris A (2011) Cationic and anionic dye adsorption by agricultural solid wastes: a comprehensive review. Desalination 280(1):1–13. https://doi.org/10.1016/j.desal.2011.07.019
63. Saleh TA, Gupta VK (2014) Processing methods, characteristics and adsorption behavior of tire derived carbons: a review. Adv Colloid Interface Sci 211:93–101. https://doi.org/10.1016/j.cis.2014.06.006
64. Balarak D, Jaafari J, Hassani G, Mahdavi Y, Tyagi I, Agarwal S, Gupta VK (2015) The use of low-cost adsorbent (canola residues) for the adsorption of methylene blue from aqueous solution: isotherm, kinetic and thermodynamic studies. Colloids Interface Sci Commun 7:16–19. https://doi.org/10.1016/j.colcom.2015.11.004
65. Kuleyin A (2007) Removal of phenol and 4-chlorophenol by surfactant-modified natural zeolite. J Hazard Mater 144(1):307–315. https://doi.org/10.1016/j.jhazmat.2006.10.036
66. Hong G-B, Yu T-J, Lee H-C, Ma C-M (2021) Using rice bran hydrogel beads to remove dye from aqueous solutions. Sustainability. https://doi.org/10.3390/su13105640
67. Dutta T, Kim T, Vellingiri K, Tsang DCW, Shon JR, Kim K-H, Kumar S (2019) Recycling and regeneration of carbonaceous and porous materials through thermal or solvent treatment. Chem Eng J 364:514–529. https://doi.org/10.1016/j.cej.2019.01.049
68. Wang Y, Wei X, Zhang R, Wu Y, Farid MU, Huang H (2017) Comparison of chemical, ultrasonic and thermal regeneration of carbon nanotubes for acetaminophen, ibuprofen, and triclosan adsorption. RSC Adv 7(83):52719–52728. https://doi.org/10.1039/C7RA08812D
69. Fanaie VR, Karrabi M, Amin MM, Shahnavaz B, Fatehizadeh A (2017) Biosorption of 4-chlorophenol by dried anaerobic digested sludge: artificial neural network modeling, equilibrium isotherm, and kinetic study. Int J Environ Sci Technol 14(1):37–48. https://doi.org/10.1007/s13762-016-1139-4
70. Kuśmierek K, Zarębska K, Świątkowski A (2016) Hard coal as a potential low-cost adsorbent for removal of 4-chlorophenol from water. Water Sci Technol 73(8):2025–2030. https://doi.org/10.2166/wst.2016.046
71. Gholizadeh A, Kermani M, Gholami M, Farzadkia M (2013) Kinetic and isotherm studies of adsorption and biosorption processes in the removal of phenolic compounds from aqueous solutions: comparative study. J Environ Health Sci Engineer 11(1):29. https://doi.org/10.1186/2052-336X-11-29
72. Liu S, Wang J, Huang W, Tan X, Dong H, Goodman BA, Du H, Lei F, Diao K (2019) Adsorption of phenolic compounds from water by a novel ethylenediamine rosin-based resin: interaction models and adsorption mechanisms. Chemosphere 214:821–829. https://doi.org/10.1016/j.chemosphere.2018.09.141
73. Kurniawan TA, Waihung L, Repo E, Sillanpää MET (2010) Removal of 4-chlorophenol from contaminated water using coconut shell waste pretreated with chemical agents. J Chem Technol Biotechnol 85(12):1616–1627. https://doi.org/10.1002/jctb.2473
74. Bilgili MS (2006) Adsorption of 4-chlorophenol from aqueous solutions by xad-4 resin: Isotherm, kinetic, and thermodynamic analysis. J Hazard Mater 137(1):157–164. https://doi.org/10.1016/j.jhazmat.2006.01.005
75. Kuśmierek K, Świątkowski A (2015) The influence of an electrolyte on the adsorption of 4-chlorophenol onto activated carbon and

multi-walled carbon nanotubes. Desalin Water Treat 56(11):2807–2816. https://doi.org/10.1080/19443994.2014.965221
76. Chen C, Geng X, Huang W (2017) Adsorption of 4-chlorophenol and aniline by nanosized activated carbons. Chem Eng J 327:941–952. https://doi.org/10.1016/j.cej.2017.06.183